1

Reliability and Durability of Thermoelectric Materials and Devices: Present Status and Strategies for Improvement

Congcong XU[1,*], Hongjing SHANG[1,2,*], Zhongxin LIANG[1,*], Fazhu DING[2], and Zhifeng REN[1]

[1] Department of Physics and Texas Center for Superconductivity (TcSUH), University of Houston, USA

[2] Key Laboratory of Applied Superconductivity, Institute of Electrical Engineering, Chinese Academy of Sciences, Beijing, China

**These authors contributed equally to this chapter.*

1.1. Introduction

The performance of a thermoelectric material is usually evaluated by its operating temperature (T) and three other interrelated parameters: electrical conductivity (σ), Seebeck coefficient (S) and thermal conductivity (k). These parameters together determine the thermoelectric dimensionless figure of merit (zT), $zT = \frac{S^2\sigma}{\kappa}T$. The thermoelectric conversion efficiency is

Thermoelectric Micro/Nano Generators 2,
coordinated by Hiroyuki AKINAGA, Atsuko KOSUGA,
Takao MORI and Gustavo ARDILA.

dependent on the *zT*. Theoretically, higher *zT* values can guarantee higher thermoelectric conversion efficiency, so there has been a great effort to improve *zT* over the past several decades, and the *zT* of some materials has been reported exceeding 2. Nevertheless, the development of thermoelectric devices has been somewhat lagging in comparison to the performance optimization of materials.

Additional scientific and engineering challenges are faced during thermoelectric device development, including long-term material stability, material parameter matching, contact layer selection, device structure and thermoelectric system design, etc. Among these challenges, stability is a prerequisite for the actual application of materials. Since thermoelectric devices are operated under large temperature differences, the environment faced by thermoelectric materials, especially in thermoelectric power generators, is relatively harsh. Repeated thermal cycles, thermal shocks and high temperatures will not only reduce the thermomechanical properties of a material but may also change its composition, which ultimately leads to deterioration in the thermoelectric performance and even complete device failure. In addition, the potential thermal stress caused by repeated thermal expansion and contraction imposes more stringent requirements on the stability of the device interface and the thermomechanical matching of the p- and n-type materials. Unfortunately, in comparison to the effort to improve *zT*, less attention has been paid to the stability issue for thermoelectric materials and devices, limiting their practical application.

Here, we will highlight this issue and bridge the gap between thermoelectric research and actual applications by discussing the durability and reliability challenges of both thermoelectric materials and devices. We first address the thermal stability of several thermoelectric materials and strategies for thermal stability improvement. Secondly, we analyze in detail thermoelectric device design, including thermal stress and interface issues. Finally, we summarize recent progress in the design and fabrication of reliable and durable thermoelectric modules and provide an outlook for future research needs.

1.2. Thermoelectric material stability

For actual applications, a material's stability is at least as critical as its thermoelectric properties, if not more important. Different kinds of instability, including component decomposition, elemental evaporation and phase transition, can result in the degradation of thermoelectric material performance, further leading to the decreased energy-conversion efficiency of thermoelectric modules. In the following section, typical instability issues of several materials with decent thermoelectric performances are discussed in detail. Strategies that have been used to improve the thermal stability of these materials are also summarized and discussed.

1.3. $Mg_3(Sb, Bi)_2$

$Mg_3(Sb, Bi)_2$ exhibits a $CaAl_2Si_2$-type crystal structure consisting of an octahedrally coordinated Mg^{2+} cation layer and a tetrahedrally coordinated anion structure $[(Mg_2Sb_2)^{2-}]$ (Shuai et al. 2017a; Song et al. 2019; Mao et al. 2018). It had long been considered a p-type semiconductor with undistinguished performance, but Te-doped n-type $Mg_3(Sb, Bi)_2$-based alloys were recently reported to show high thermoelectric performance, demonstrating good potential for both power generation and cooling applications (Tamaki et al. 2016; Zhang et al. 2017). Subsequently, various strategies, including tuning the carrier scattering mechanism (Mao et al. 2017a; Shuai et al. 2017b), defect engineering (Mao et al. 2017b; Li et al. 2019, 2020a) and doping (Shi et al. 2019b, 2019c; Shu et al. 2019), have been successfully applied in Mg_3Sb_2-based alloys, achieving a state-of-the-art average zT value up to 1.1 in the range of 300~500 K (Imasato et al. 2019a; Shi et al. 2019a; Shang et al. 2020a; Wood et al. 2019).

Among all defects in Mg_3Sb_2-based materials, Mg vacancies have the lowest defect formation energy around the Fermi level, thus resulting in the intrinsically high concentration of Mg vacancies causing p-type conduction of these materials (Zhang et al. 2019). The addition of extra Mg into the matrix has been reported to be successful in reducing the Mg-vacancy concentration and achieving n-type conduction (Shuai et al. 2018; Kuo et al. 2019). At the operating temperature of 773 K, the corresponding vapor pressures of elemental Mg, Sb and Bi are 7,390 Pa, 139 Pa and 9.64 Pa,

respectively. Such a great difference in vapor pressure will result in significant Mg loss at high temperatures. Jørgensen et al. (2018) studied the thermal stability of $Mg_3Sb_{1.475}Bi_{0.475}Te_{0.05}$ via high-temperature synchrotron powder X-ray diffraction and found that a Bi impurity phase forms in thermal cycles from 300 K to 725 K, suggesting the compound's high-temperature structural instability. Shang et al. (2020b) reported that $Mg_3Sb_{2-x}Bi_x$ alloys ($Mg_{3.2}Sb_{1.5}Bi_{0.49}Te_{0.01}$, $Mg_{3.2}SbBi_{0.99}Te_{0.01}$ and $Mg_{3.2}Sb_{0.49}Bi_{1.5}Te_{0.01}$) showed performance degradation at 673 K and 773 K via long-term in situ measurements of their thermoelectric properties, although they demonstrated the stable electrical properties of these compounds at 573 K, as shown in Figure 1.1. It can be seen that the Seebeck coefficient of $Mg_{3.2}Sb_{0.49}Bi_{1.5}Te_{0.01}$ crosses over from negative values (n-type) to positive values (p-type) at 773 K, which has been attributed to the Mg loss notable by microstructural analysis and results in the formation of Mg vacancies that pin the Fermi level, eventually enabling the p-type conduction. Fortunately, coating the surfaces of the $Mg_3Sb_{2-x}Bi_x$ alloys with boron nitride was found to significantly improve their thermal stability by effectively limiting Mg loss at high temperatures. The time-dependent Hall carrier concentration of $Mg_3Sb_{2-x}Bi_x$ with cationic doping by La (Imasato et al. 2018), Yb (Wood et al. 2020) and Y (Shi et al. 2019c) at high temperatures and in a dynamic vacuum was also explored, and the cation-doped samples showed a delayed decrease in the carrier concentration compared with their Te-doped counterparts, indicating that doping with a cation rather than with Te can also improve the thermal stability of $Mg_3Sb_{2-x}Bi_x$ to some extent. Considering the large differences in the vapor pressures of the elements in $Mg_3Sb_{2-x}Bi_x$, high-temperature Mg loss that results in structural instability and decreased thermoelectric performance is common, thus restricting the operating temperature ranges of these materials. This disadvantage overshadows the high-temperature zT values and makes practical applications less appealing at temperatures higher than 673 K. Therefore, determining how to improve the thermal stability of $Mg_3Sb_{2-x}Bi_x$ compounds is more significant than simply focusing on enhancing their zT values.

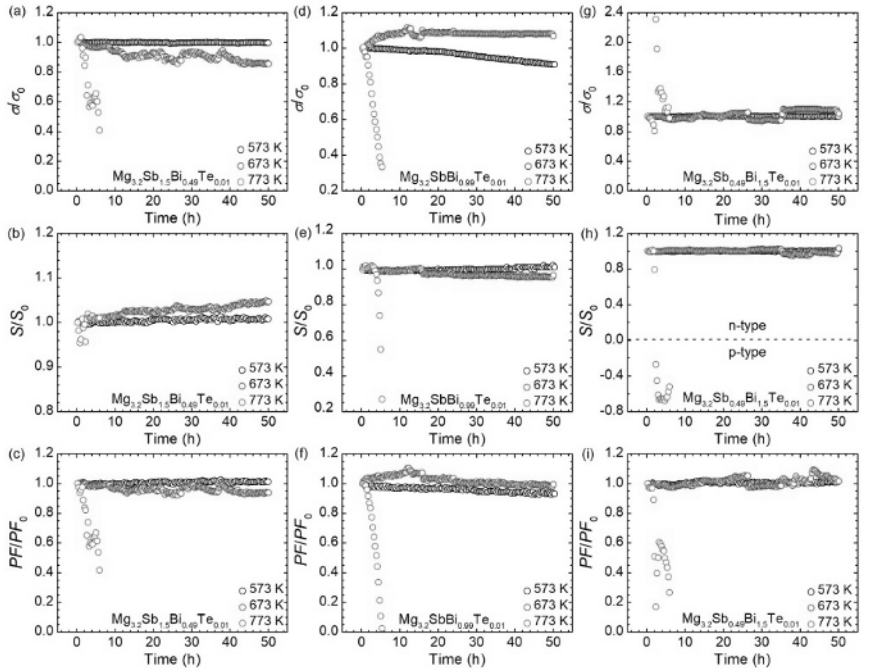

Figure 1.1. *Long-term in situ measurement of thermoelectric properties of $Mg_3Sb_{2-x}Bi_x$ alloys at 573 K, 673 K and 773 K. (a)–(c) σ/σ_0, (d)–(f) S/S_0 and (g)–(i) PF/PF_0 for $Mg_{3.2}Sb_{1.5}Bi_{0.49}Te_{0.01}$, $Mg_{3.2}SbBi_{0.99}Te_{0.01}$ and $Mg_{3.2}Sb_{0.49}Bi_{1.5}Te_{0.01}$, respectively. σ_0, S_0 and PF_0 represent the initial values; σ, S and PF represent the measured values at the specified time. Reprinted from Shang et al. (2020b). For a color version of this figure, see www.iste.co.uk/akinaga/thermoelectric2.zip*

1.4. Zn_4Sb_3

β-Zn_4Sb_3 is a well-known p-type thermoelectric material for applications in the intermediate temperature range (473~673 K) and exhibits high zT values up to 1.3 at 673 K (Zou et al. 2015). The high thermoelectric performance of β-Zn_4Sb_3 and its good potential for thermoelectric applications mainly result from its low lattice thermal conductivity (~0.3 W m^{-1} K^{-1} above 500 K), which is largely caused by its disordered structure that includes interstitial Zn (Dasgupta et al. 2013).

However, with the increasing temperature, β-Zn_4Sb_3 starts to decompose at 473 K due to a loss of Zn, forming ZnSb and Zn as decomposition

productions and degrading its thermoelectric performance (Hao et al. 2011; Yang et al. 2017a, 2017b). Thus, it is of great significance to improve the thermal stability of β-Zn_4Sb_3 for practical applications. Based on both experimental results and theoretical calculations, doping with heavier metals can hamper the Zn migration and subsequently freeze β-Zn_4Sb_3 in its local disordered structure, eventually improving its thermal stability. It has also been found that this doping strategy can optimize the compound's electrical properties. For example, Wang et al. reported that Pb-doped β-Zn_4Sb_3 shows increased carrier mobility, achieving an optimized zT value of ~1.2 at 660 K (Wang et al. 2012), while its thermal stability is clearly improved due to the decreased Zn evaporation at high temperatures. Similar results were also reported by Deng et al. (2017). Furthermore, the addition of any of Ag (Song et al. 2018), Cd (Yin et al. 2010), Ge (Moghaddam et al. 2019), In/Sn (Shai et al. 2015), ZnO (Tang et al. 2015), etc. into β-Zn_4Sb_3 can also simultaneously improve its thermoelectric performance and high-temperature stability.

1.5. Skutterudites

In recent years, skutterudite-based materials have attracted significant attention due to their outstanding performance over a wide temperature range and their relatively inexpensive constituent elements. Among the various kinds of skutterudites, $CoSb_3$, a diamagnetic (Co^{3+}, $3d^6$) narrow-bandgap semiconductor, demonstrates high carrier mobility and a relatively large effective electron mass. Generally, $CoSb_3$-based thermoelectric generators can operate at temperatures up to 773 K. However, a series of studies have revealed that $CoSb_3$-based skutterudites undergo oxidation and Sb sublimation when the operating temperature exceeds 673 K, resulting in short service life (Sales et al. 1996; Zhang et al. 2016; Liu et al. 2020). Therefore, effective and reliable approaches are needed to address these instability issues.

The most effective method reported thus far is physical isolation, or inhibiting the sublimation of elements by spraying on a protective coating such as metal (El-Genk et al. 2006), ceramic (Zhang et al. 2016; Chen et al. 2013), glass (Dong et al. 2012), aerogel (Sakamoto et al. 2008) or a multilayered composite (Xia et al. 2014; Zhang et al. 2016). Introduction of the coating under certain conditions can indeed improve the stability of $CoSb_3$-based skutterudites at high temperatures, but it may result in some new problems at the same time. For example, the diffusion of a metal

coating into the thermoelectric legs may result in decreasing performance over increasing thermal cycles (Dong et al. 2012). Moreover, the metal coating would cause an electrical short in actual applications. Although aerogel coating is highly robust and resistant to high temperatures, it could include micropores that may serve as escape channels for elemental oxidation and sublimation. Coating with another material such as glass or a ceramic may result in a mismatch of coefficient of thermal expansion (CTE) values or poor adhesion strength. Thus, coating with a multilayered structure consisting of different kinds of material is proposed. Zhang et al. (2016) reported a more effective multilayered coating with Mo, SiO_x and glass-ceramic layers. As shown in Figure 1.2, compared with samples without coating and with single-layered coating, that with the multilayered coating exhibits better stability in air at 873 K, indicating the effective suppression of both oxidation and sublimation. Nevertheless, suppressing decomposition in and improving the stability of skutterudite-based materials remain very challenging in practical application scenarios.

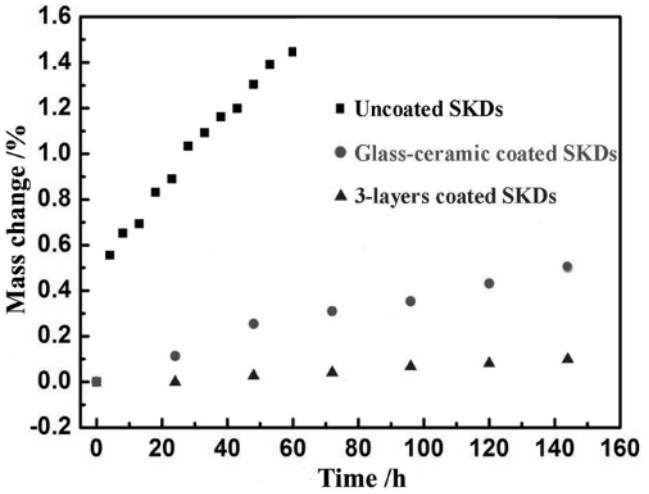

Figure 1.2. *Mass change of coated and uncoated skutterudites at 873 K in air as a function of time. Reprinted from Zhang et al. (2016). For a color version of this figure, see www.iste.co.uk/akinaga/thermoelectric2.zip*

1.6. $Cu_{2-x}X$ (X = S, Se, Te)

Copper chalcogenides $Cu_{2-x}X$ (X = S, Se, Te) possess complex atomic arrangements, and the Cu-deficient region in the Cu–Se system ($Cu_{2-x}Se$)

exhibits two distinct phases, a low-temperature α phase and an intermediate-temperature β phase (Liu et al. 2012). The low-temperature α phase with a low-symmetry crystal structure, where the Cu atoms are ordered and not superionic, is stable up to ~400 K and eventually transitions to the intermediate-temperature β phase with a cubic structure at ~400 K. In the β phase, the superionic Cu ions are kinetically disordered, leading to its remarkably low thermal conductivity and high thermoelectric performance. Significant advances have recently been obtained in studies of the p-type $Cu_{2-x}Se$ materials, and the zT value reportedly reaches 2.4 at 1,000 K for $Cu_{2-x}Se$/carbon nanotube (CNT) hybrid materials, showing promise for applications (Nunn et al. 2017, Lu et al. 2020b, Zhang et al. 2020b).

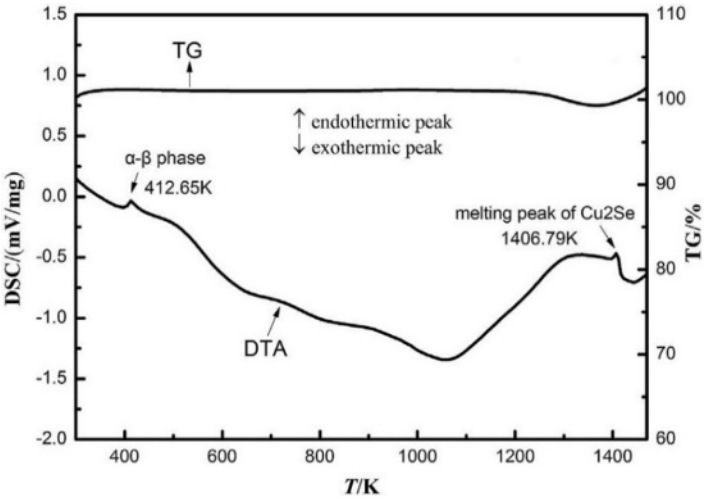

Figure 1.3. *TG-DTA curves for single-crystal Cu_2Se with a heating rate of 10 K/min. Reprinted from Liu et al. (2019)*

Unfortunately, $Cu_{2-x}Se$ materials suffer from thermal instability issues when they are applied at a high temperature and exposed to a large current, limiting their application in large-scale thermoelectric power generation (Shi et al. 2020). Thus, it is urgent to find out the mechanism of the instability issues of $Cu_{2-x}Se$ materials and improve their performance liability. Bohra et al. (2016) studied the effects of thermal cycles on the thermoelectric properties of $Cu_{2-x}Se$ in the temperature range of 320~1,070 K and found that electrical resistance increased with increasing thermal cycles, resulting in a reduction in the power factor from 13 μW cm^{-1} K^{-2} for the first cycle to

8 μW cm^{-1} K^{-2} for the third cycle at ~1,070 K. This change was attributed to Se loss and phase transition with increasing thermal cycles. Xue et al. (2019) reported that a high synthesis temperature not only enhances the thermoelectric performance of $Cu_{2-x}Se$ but also effectively improves its thermal stability; specifically, the Seebeck coefficient, electrical conductivity and thermal conductivity were found to be nearly constant between the heating and cooling cycles over the temperature range of 300~723 K for a sample fabricated at 1,273 K. Furthermore, a Ni/Mo/$Cu_{1.96}Se_{0.8}S_{0.2}$ thermoelectric unileg was able to exhibit a very steady power output over 400 thermal cycles between 473 K and 873 K through the control of its chemical composition (Mao et al. 2019b). Other dopants, such as Li (Kang et al. 2017), CNTs (Nunn et al. 2017), W (Bohra et al. 2020) and Cd (Lu et al. 2020a), can also improve the thermal stability of $Cu_{2-x}Se$ materials, allowing them to be applied for power generation. Additionally, single-crystal α-$Cu_{2-x}Se$ was fabricated using the Bi-flux method and no weight loss occurred below the melting point (~1,403 K), as shown by the thermogravimetric-differential thermal analysis (TG-DTA) results displayed in Figure 1.3. The DTA curve shows the endothermic peak at ~400 K, which has been attributed to the Cu_2Se α–β phase transformation. The power factor of the single-crystal samples did not obviously decrease after three thermal cycles in the temperature range of 300~690 K, demonstrating their improved thermal stability compared with the polycrystalline materials (Liu et al. 2019). However, single crystals are usually more expensive than the polycrystalline materials, so they are not preferred for large-scale applications.

1.7. GeTe

GeTe-based thermoelectric materials were first studied in the 1960s, and they re-emerged as a subject of research interest only recently. Thanks to band engineering and defect engineering strategies, the zT values exceeding 2 have been achieved in GeTe-based materials, showing their promise for applications (Hong et al. 2020; Zhang et al. 2020a). Nevertheless, the actual application of GeTe-based modules have a major obstacle to overcome concerning how the pristine GeTe undergoes a reversible transition between a low-temperature rhombohedral structure and a high-temperature cubic structure around 700 K, as illustrated in Figure 1.4. It should be noted that such structural instability can seriously reduce the reliability of devices if it is not handled properly. Additionally, there is a considerable change in the coefficient of thermal expansion (CTE) between the two phases

(11.2×10^{-6} K^{-1} for the rhombohedral structure and 23.4×10^{-6} K^{-1} for the cubic structure), and such CTE change is extremely detrimental in device applications since it can cause significant thermal stress during operation (Xing et al. 2021). Thus, methods to suppress the phase transition are required.

Fortunately, Liu et al. (2018) successfully obtained GeTe-based material that is in the cubic phase over the entire operating temperature range through simple Mn and Bi co-doping at the Ge site. Soon afterwards, Zheng et al. (2018) reported that the lower-temperature cubic GeTe can also be achieved by Mn and Sb co-doping and found that the transition temperature was reduced from 700 K closer to room temperature. The above two studies show that Mn plays a significant role in inhibiting the phase transition. Bi and Sb can also adjust the crystal structure to a certain extent, but they are more responsible for regulating the carrier concentration. Recently, resonant bonding properties induced by a symmetrized crystal lattice were found in the Ti-doped GeTe-based material (Li et al. 2020c). Ti doping not only can reduce the lattice constant c/a ratio to achieve a cubic structure but can also enhance the Seebeck coefficient due to the increased band degeneracy (Shuai et al. 2019).

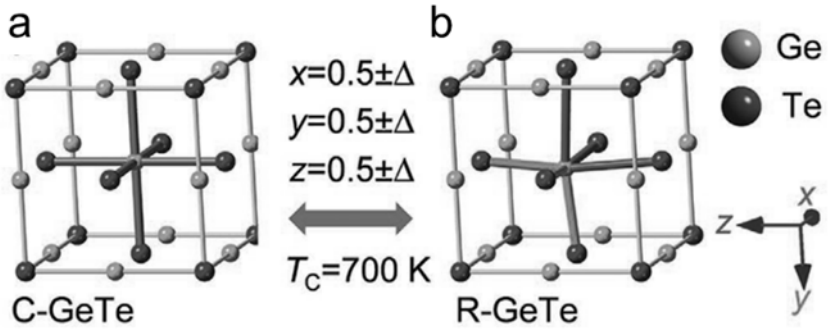

Figure 1.4. *Structure of GeTe: (a) cubic and (b) rhombohedral. Reprinted from Li et al. (2021). For a color version of this figure, see www.iste.co.uk/akinaga/thermoelectric2.zip*

1.8. Outlook on thermoelectric materials stability

Admittedly, the instability issue is universal in thermoelectric materials because of their weak chemical bonding and highly disordered content. In this section, different typical instability issues faced by several kinds of

materials were briefly introduced, and the corresponding strategies to address these issues were also discussed in detail. In addition to the above-discussed thermoelectric materials, other promising materials with excellent thermoelectric performance, including PbTe (Wang et al. 2018), BiCuSeO (Li et al. 2014) and half-Heuslers (Rausch et al. 2016), also suffer from thermal instability, which markedly impedes their commercial applications, especially for the generation of thermoelectric power. Generally, the instability issue can be solved either chemically or physically. From a chemical point of view, doping or heat treatment can improve the stability of a thermoelectric material's constituent elements and structure on a microscopic level. For some special materials with phase transitions, reasonable chemical doping can alter the phase-transition point, thereby avoiding the instability of the material in the operating temperature range. From a physical point of view, isolating a material from the external environment, such as with a coating or through vacuum packaging, is also an effective measure to effectively enhance its stability. These strategies should be thoroughly evaluated and rationalized in future studies with the help of advanced characterization tools and theoretical simulations. Without these methods, it would be difficult to understand the origin of phase-transition regulation or structure-stability preservation when introducing external dopants. In addition, for long-term stability, developing a rapid and scalable method for preparing thermoelectric materials with fewer defects is advantageous. In short, to achieve the practical uses of thermoelectric materials, greater efforts should be made with enhancing the thermal stability of existing materials and searching for new materials with both high performance and good stability. In particular, reporting the stability data of high-zT materials together with their transport property measurements is recommended for at least the papers on device performance.

1.9. Thermoelectric device design analysis

1.9.1. *Thermal stress analysis*

Despite the tremendous improvements in thermoelectric material performance over the last several decades, research into building thermally and mechanically reliable devices has been very slow. Since thermoelectric modules are subjected to large temperature gradients over long periods, the thermomechanical properties and thermal stability of various constituent components must be considered in device design and manufacturing (Karri et al. 2018). Significant thermal stress, deformation and even failure may

occur in thermoelectric devices due to mismatches in the thermal, mechanical and rheological properties of the constituent components caused by material specificity, cyclic thermal loading and possible mechanical vibration (Music et al. 2016). As a result, in designing a thermoelectric device, it is critical to conduct temperature distribution and thermal stress analyses in order to effectively reduce thermal stress through material selection or structure optimization. The main aim of such a thermomechanical stress study is to maintain the thermoelectric device's high output performance under a long-term operation.

In this section, thermomechanical stress in thermoelectric modules is discussed in depth. We first discuss the coefficient of thermal expansion, which is a significant factor in determining thermal stress, as well as other design considerations relevant to thermal stress, including module configuration and geometry. We then present an analysis of the lowest value of thermal conductivity based on the maximum allowable thermal shear stress, emphasizing the importance of balancing the high zT generated by phonon scattering with mechanical reliability. These analyses elucidate the relationship between the above factors and the performance, reliability and durability of thermoelectric devices, shedding light on the optimal design of reliable thermoelectric devices.

1.9.1.1. *Coefficient of thermal expansion (CTE)*

The coefficient of thermal expansion (CTE, α) of a material is its length change in response to temperature variation. Differing expansion of constituent parts of a thermoelectric device under a considerable temperature gradient would result in high thermal stress and hence a greater risk of interfacial damage during long-term operation (He et al. 2018). For example, cracking or exfoliation at the interface of an oxide-based module is due to the widely differing CTEs of oxides and metallic contact materials (Liu et al. 2015).

The temperature-gradient-induced mechanical stress $\xi(T)$ of a thermoelectric material can be approximated by:

$$\xi(T) = \frac{\alpha(T)E(T)\Delta T}{(1-\nu(T))} \qquad [1.1]$$

where α, E and ν are its CTE, Young's modulus and Poisson's ratio, respectively (Ni et al. 2013).

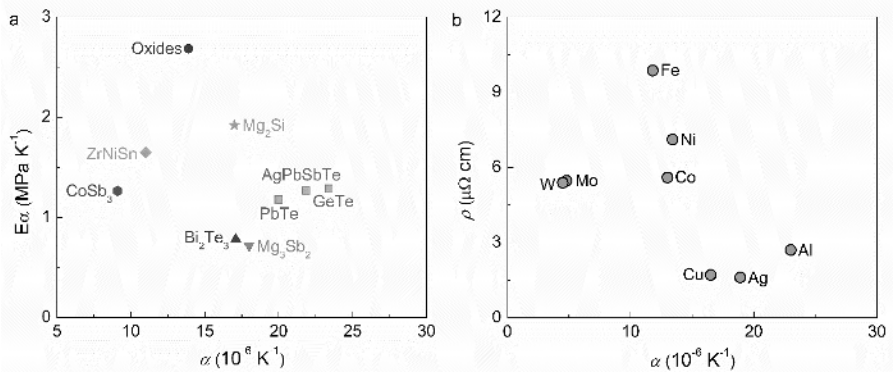

Figure 1.5. *(a) Coefficient of thermal expansion (CTE, α) and elastic modulus-CTE product (Eα) for representative thermoelectric materials. Data obtained from Ni et al. (2013), Zhao and Tan (2014) and Music et al. (2016). (b) CTE and electrical conductivity (r) for pure metals. Data obtained from Chowdhury et al. (2009). For a color version of this figure, see www.iste.co.uk/akinaga/thermoelectric2.zip*

Clearly, a large CTE value and a high Young's modulus are undesirable for reduced thermal stress. According to calculation results, a CTE mismatch between different components in a thermoelectric module can result in excessive thermal stress and in situ fracture (Ravi et al. 2009). In other words, CTE has a significant impact on the module's thermomechanical robustness. Hence, obtaining thermal expansion statistics for commonly used thermoelectric materials and investigating the underlying relationship between the structure and the thermal expansion coefficient of each are critical for achieving thermally match systems in thermoelectric devices. The measured CTE results for commonly investigated thermoelectric materials with high zT values are summarized in Figure 1.5a. Clearly, most high-performance thermoelectrics have CTE values of more than 15×10^{-6} K^{-1}, which can be attributed to the weak chemical bonding in these materials that also results in their low lattice thermal conductivity. The large CTE values emphasize the importance of selecting appropriate metal electrodes and designing reliable contact layers for the thermoelectric legs in a module in order to reduce thermal stress (Ni et al. 2013). Additionally, the CTE values of thermoelectric compounds should be optimized to establish better matches between p- and n-type materials or between thermoelectric materials and electrodes by tuning the compositions, filler atoms, grain sizes (Rogl et al. 2017) and additives (Rogl et al. 2010). However, these solutions

need to be carefully examined to ensure that high zT values are retained. The CTE and electrical conductivity values of pure metals are shown in Figure 1.5b as a reference to choose suitable contact layers for both CTE matching and low electrical resistivity. Music et al. (2016) used the first-principles calculation method to investigate the thermomechanical response of 20 thermoelectrics. They found that oxides exhibit larger products of linear thermal expansion coefficient and elastic modulus, implying that thermoelectric oxides are susceptible to thermally induced stress, shock and fatigue. For convenience in prediction and matching, it was also suggested that equilibrium volume, an easily measurable parameter, can be used to estimate this product and the thermal response of thermoelectric materials.

1.9.1.2. *Module configuration and geometry design*

Realizing high conversion efficiency or output power density in a thermoelectric module relies on a specific configuration and geometry, so its fabrication always involves the design and optimization of these factors (Wu et al. 2014). The principle of thermoelectric device configuration design is to minimize the internal stress caused by temperature difference and thermal shock while making full use of the heat source.

The π-shaped, O-shaped and Y-shaped structures, schematically illustrated in Figure 1.6, are the most common thermoelectric-module configurations (Zhang et al. 2016). In a typical π-shaped module as shown in Figure 1.6a, many thermoelectric unicouples consisting of an n-type leg and a p-type leg are connected electrically in series and thermally in parallel. In order to maximize the use of temperature differences, the direction of heat flow is usually perpendicular to the substrate. It should be noted that when this design is applied at higher temperatures, the thermally induced stress, expansion and diffusion of different materials should be thoroughly considered because the repeated heat shock may cause severe deformation and even device failure, especially at the contacts. An O-shaped module (Figure 1.6b) consists of a coaxial assembly of many annular flat gaskets consisting of alternating n- and p-type thermoelectric rings. Compared to the π-shaped configuration, the O-shaped configuration makes it easier to achieve device integration, efficient heat transfer and low-stress structure design, but the manufacturing and joining technology needed for the specially shaped thermoelectric elements and the metal electrodes is very difficult to master if not impossible. The Y-shaped module configuration (Figure 1.6c) has been designed mainly to eliminate the impact of thermal expansion mismatch between different constituent components while

maintaining excellent thermoelectric performance. In this configuration, rectangular n- and p-type thermoelectric materials are alternately connected to electrode plates in a sandwich structure, which allows the thermoelectric elements to be maintained in a non-fully constrained state and reduces the thermal expansion and deformation caused by the constraints of the hot and cold sides. The horizontal series connection of the n- and p-type materials also avoids the stress concentration caused by the difference in their thermal expansion coefficients.

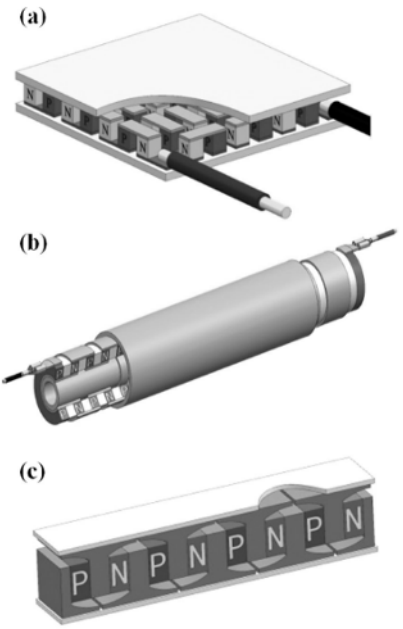

Figure 1.6. *Schematic diagrams of (a) π-shaped, (b) O-shaped and (c) Y-shaped modules. Reprinted from Zhang et al. (2016). For a color version of this figure, see www.iste.co.uk/akinaga/thermoelectric2.zip*

In addition to the shape of the module, the unicouple geometry plays an important role in maximizing performance and maintaining it under large thermal stress (Shittu et al. 2020). Recent thermodynamic and thermal stress studies of thermoelectric generators have revealed that the highest stress level is found at the edges of a module, particularly those on its hot side (Al-Merbati et al. 2013). By tuning the pin geometry, the temperature variation can be improved, and thus the lifetime of the module can be

prolonged. Fabián-Mijangos et al. (2017) compared the effects of various leg shapes, including square, hexagon, octagon and circular prisms, on overall thermal stress and found that cylindrical legs are preferable under the fixed hot side condition, while square prisms are more reliable under the free hot side condition. Although modifying the leg dimensions can improve a module's thermal reliability, a unilateral focus on thermodynamic properties may result in low output-power performance. Erturun et al. (2015) found that there is an inverse relationship between output performance and thermal integrity by using three-dimensional finite-element analysis and experiments, indicating the importance of determining the optimal shape for balancing performance and stability. More specifically, Sarhadi et al. (2015) recommended that the thermoelectric legs should be long enough to achieve high efficiency and low thermal stress while short enough to maintain a high output power density. A segmented module presents a more complicated situation since more factors are involved in its structural optimization. In most cases, a compatibility factor match between segmented materials is sufficient to produce an effective segmented device. However, Jia et al. (2014) noted that when considering the strength requirements, a high conversion efficiency in a segmented device is not always possible. In short, multi-parameter optimization of thermoelectric generators is required to achieve both maximum efficiency and structural reliability.

Modulating the hot-side design of a thermoelectric device by taking into consideration the connection structure and heat flux direction is another strategy to reduce thermal stress and obtain a durable interface. Sun et al. (2021) examined a new design that uses a step structure of ceramic plates with thermoelectric legs inserted into them, which separates the heat and current conduction paths at the hot-side electrode (Figure 1.7). As a result, interconnect cracking is only affected by the connection between the hot-side ceramic plate and the metallic interconnect adjacent to it, which reduces the thermal stress damage of the interconnect and increases the number of operation cycles prior to failure. Additionally, the design was calculated to have a favorable impact on the module's power output performance, showing simultaneous improvement in thermomechanical stability and thermoelectric performance. In the future, a real module should be prepared and evaluated to substantiate this new design and initiate further improvements, and also to show the cost difference since the new design will be more expensive.

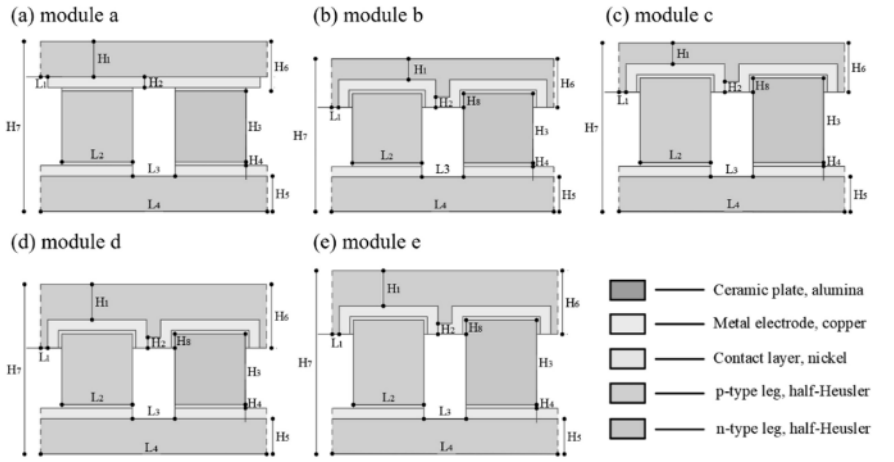

Figure 1.7. *Schematic diagrams of thermoelectric modules featuring (a) the conventional thermoelectric unicouple geometry and (b–e) the new hot-side design geometry with different parameters. Reprinted from Sun et al. (2021). For a color version of this figure, see www.iste.co.uk/akinaga/thermoelectric2.zip*

When considering the substrate design specifically, there are two main strategies for protecting the module from thermal stress. Increasing the thickness of the ceramic plates can relieve thermal stress while ensuring that the device's output performance remains nearly constant. Another effective way to reduce thermal stress is to replace rigid substrates with compliant pads for electrical insulation (Kambe et al. 2010). Nevertheless, in this case, the derived module will be mechanically weak and will need additional encapsulation. Most thermoelectric modules currently investigated use alumina substrates because of their high thermal conductivity. A Cu electrode strip can be deposited onto each substrate prior to assembly. The thickness of the Cu electrode strips can be adjusted according to the maximum expected output current of the module.

1.9.1.3. *Materials design for reduced thermal stress: engineering thermal conductivity* κ_{eng}

Decreasing lattice thermal conductivity by introducing multi-scale microstructures has been widely applied to improve the performance of thermoelectric materials. In particular, nanostructured grains are proposed to

scatter phonons significantly without degrading electrical transport, which is beneficial for the overall improvement of zT values. Intuitively, the thermoelectric performance of a material would be significantly improved if its lattice thermal conductivity could be reduced to the minimal value predicted by theoretical calculations. However, because of the corresponding weak chemical bonding and significant anharmonicity, materials with exceptionally low lattice thermal conductivity are usually brittle, limiting their practical applications. In other words, even though carrier mobility is unaffected, the low lattice thermal conductivity attained by creating vast defects may degrade mechanical strength and stability since thermoelements will be subjected to large thermal gradients and thermal stress. Thus, reconsidering the phonon scattering technique is critical to balancing zT values and mechanical brittleness. Inspiringly, Kim et al. (2016) hypothesized that when exposing materials to shear thermal stress, there is a minimal value of thermal conductivity which is safe to employ (Figure 1.8). To begin, they proposed that there is an appropriate range of leg length (L), where the lower limit of leg length (L_{min}) is dictated by the yield strength and the upper limit of leg length (L_{max}) may be computed using thermoelectric material parameters and boundary conditions. For materials with higher thermal conductivity, a larger value of L_{max} could be expected for a fixed cold-side temperature. If L_{max} is greater than L_{min}, it is safe to reduce the thermal conductivity so that L_{max} is closer to L_{min}, therefore enhancing the efficiency of the device. Engineering thermal conductivity (κ_{eng}) is the thermal conductivity value when L_{min} and L_{max} are the same. Thus, κ_{eng} can be defined as the lower limit of a material's thermal conductivity that still assures the device's thermal reliability in a steady-state operation. On the other hand, since thermoelectric devices are subjected to thermal loading and thermal shock in real applications, it is also important to investigate the minimum thermal conductivity of thermoelectric materials during transient operation, which can be estimated from the dynamic boundary conditions and the thermomechanical properties of the materials. Based on these findings, Kim et al. (2016) investigated a Bi_2Te_3-based module as a case study and found that further reduction in thermal conductivity for zT improvement should not be attempted because the thermal conductivity of current-generation p-type Bi_2Te_3 already approaches the steady-state κ_{eng}. In contrast, more reliable performance improvement may rely on boosting its electrical properties.

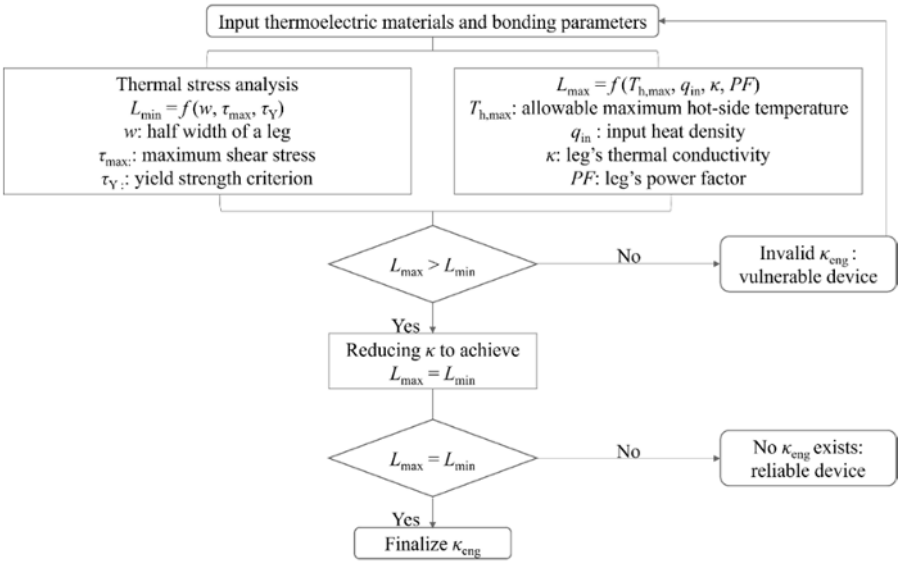

Figure 1.8. *Flow chart for calculating engineering thermal conductivity (κ_{eng}) in the steady state. Reproduced from Kim et al. (2017)*

1.9.2. *Interface analysis, design and fabrication*

The interfaces between thermoelectric materials and metal electrodes in a thermoelectric device undergo complex physical and chemical processes during operation due to repeated thermal cycling and thermal shock. In addition to the thermal stress mentioned above, more engineering problems, such as bonding strength, contact resistance and high-temperature diffusion, are confronted when considering interfaces. These issues have a great impact on the reliability and durability of the device. In the following section, the relationship between the interface properties and the device performance, as well as the failure behavior of the interfaces are first analyzed in detail, demonstrating the great importance of the interfaces. Subsequently, general selection and design principles for high-performance and reliable interfaces are introduced.

1.9.2.1. *Interface-induced performance degradation and device failure*

Contact thermal and electrical resistance at the interfaces between different components of the module will result in lower power output performance because of the wasted electricity and heat. Such a performance

discrepancy can occur at either a pristine imperfect joining or an interface that is increasingly degraded over long-term thermal cycles. In order to evaluate the effect of the interface contacts on device performance, Kim (2018) developed a numerical method for the performance analysis of thermoelectric generators with thermal and electrical contact resistance, in which the effectiveness was defined as the ratio of the thermoelectric generator's power output with any resistance to that without resistance. Effectiveness thus indicates how much of the potential performance is actually achieved in the presence of any resistance, and the corresponding mathematical results and numerical modeling for this parameter are shown in Figure 1.9. It is clear that the effectiveness increases with increasing thermal contact conductance (i.e. decreasing thermal contact resistance) and decreases with increasing electrical contact resistivity. According to the numerical simulation, low contact thermal conductance can cause performance degradation of up to ~30%, while large electrical contact resistivity can cause performance degradation of more than 40%. The results of this study emphasize the importance of interfaces on the actual performance of thermoelectric generators.

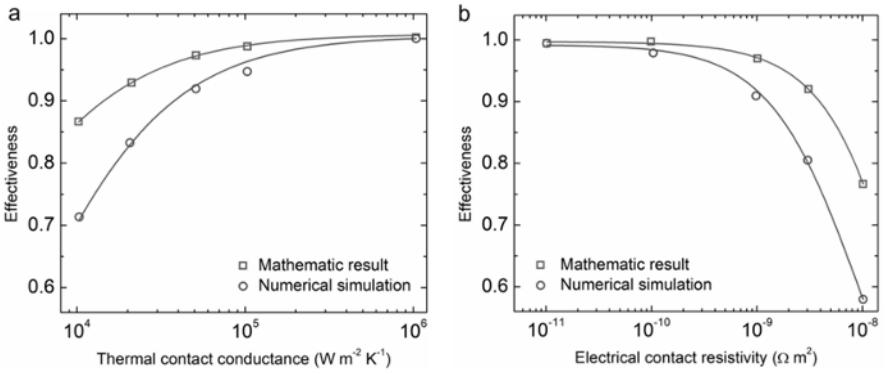

Figure 1.9. *Effect of (a) thermal contact conductance and (b) electrical contact resistivity on thermoelectric device performance. Data obtained from Kim (2018). For a color version of this figure, see www.iste.co.uk/akinaga/thermoelectric2.zip*

For thermoelectric cooling devices, the theoretical value of the coefficient of performance (COP) without considering thermal or electrical contact can be obtained by the formula:

$$\mathrm{COP} = \frac{T_\mathrm{c}}{T_\mathrm{h} - T_\mathrm{c}} \frac{\sqrt{1 + \overline{ZT}} - \frac{T_\mathrm{h}}{T_\mathrm{c}}}{\sqrt{1 + \overline{ZT}} + 1}. \qquad [1.2]$$

This formula is based on the theory developed by Ioffe in 1957 and is not highly accurate in evaluating thermoelectric modules (Ioffe 1957). In 1996, Rowe and Min proposed a more complete method, in which the thermal and electrical contacts are considered (Rowe 1995). The output voltage V and current I can be expressed by:

$$V = \frac{NS(T_\mathrm{h} - T_\mathrm{c})}{1 + \frac{2\kappa l_\mathrm{c}}{\kappa_\mathrm{c} l}}, \qquad [1.3]$$

and

$$I = \frac{AS(T_\mathrm{h} - T_\mathrm{c})}{2\rho(\frac{2\rho_\mathrm{c}}{\rho} + l)(1 + \frac{2\kappa l_\mathrm{c}}{\kappa_\mathrm{c} l})} \qquad [1.4]$$

where N, S, A, l, l_c, κ, κ_c, ρ and ρ_c are the number of thermocouples in the module, the Seebeck coefficient, the cross-sectional area of the thermoelectric material, the length of the thermoelectric leg, the thickness of contact layer, the thermal conductivity of the thermoelectric leg and of the contact layer and the electrical resistivity of the thermoelectric leg and of the contact layer, respectively. $\kappa_\mathrm{ratio} = \kappa / \kappa_\mathrm{c}$ and $\rho_\mathrm{ratio} = 2\rho_\mathrm{c} / \rho$ are standard thermal and electrical contact parameters, respectively. Generally, $\kappa_\mathrm{ratio} \sim 0.2$ and $\rho_\mathrm{ratio} \sim 0.1$ mm are appropriate values for commercially available Peltier modules. The modified conversion efficiency $\mathrm{COP}_\mathrm{rev}$ can be derived as:

$$\mathrm{COP}_\mathrm{rev} = \frac{(T_\mathrm{h} - T_\mathrm{c}) / T_\mathrm{h}}{(l + 2\kappa_\mathrm{ratio} \frac{l_\mathrm{c}}{l})^2 \{(2 - \frac{1}{2}[(T_\mathrm{h} - T_\mathrm{c}) / T_\mathrm{h}] + (4 / ZT_\mathrm{h})[(1 + \rho_\mathrm{ratio}) / (1 + 2\kappa_\mathrm{ratio} l_\mathrm{c})]\}}, \qquad [1.5]$$

where $Z = S^2/\rho\lambda$. COP_{rev} could be further derived for operation in the Peltier mode:

$$COP_{rev} = \frac{l}{l + 2\kappa_{ratio} l_c} \left(\frac{T_c}{T_h - T_c} \frac{\left[1 + \frac{Z\overline{T}l}{\rho_{ratio} + l}\right]^{1/2} - \frac{T_h}{T_c}}{\left[1 + \frac{Z\overline{T}l}{\rho_{ratio} + l}\right]^{1/2} + 1} - \frac{\kappa_{ratio} l_c}{l} \right), \quad [1.6]$$

where $\overline{T}$ is the mean temperature across the thermoelectric module. Based on this formula, the relationship between COP_{rev} and the length of the thermoelectric material at different κ_{ratio} and ρ_{ratio} values is shown in Figure 1.10 for $l_c = 0.5$ mm, $Z = 2\times10^{-3}$ K^{-1} and $\Delta T = 25$ K with T_h at 300 K. It is clear that COP_{rev} varies under different κ_{ratio} and ρ_{ratio} values. The COP_{rev} of a 1-mm leg increases by ~18.6% when κ_{ratio} decreases from 0.1 to 0.001 (i.e. the thermal conductivity of the contact layer increases), while it decreases by ~12.6% when ρ_{ratio} increases from 0.1 mm to 0.2 mm (i.e. the electrical resistivity of the contact layer increases). A dramatic decrease can be observed in COP_{rev} when the length of the thermoelectric leg is less than 2 mm. The thermal and electrical resistance of the contact layer become increasingly more important once the length of the thermoelectric leg is relatively short. Therefore, in thermoelectric cooling devices, for which the service environment is not as harsh as that for the thermoelectric generators, a relatively slight increase in contact resistance still leads to notable degradation in the cooling performance.

In actual applications, device failure frequently occurs at the interfaces which undergo repeated thermal shocks, which place greater demands on the interfaces. Figure 1.11 shows the results of long-term thermal stability testing of a $MnSi_{1.77}/Mg_2Si_{1-x}Sn_x$-based thermoelectric module (Mejri et al. 2020) and a Bi_2Te_3-based thermoelectric leg (Barako et al. 2012). For the $MnSi_{1.77}/Mg_2Si_{1-x}Sn_x$-based thermoelectric generator, the thermoelectric legs were soldered to metalized ceramic plates using silver, as shown in Figure 1.11a. The barrier layer between the legs and the solder consists of a

thin layer of Au/Ti (300/100 nm). During testing, thermal cycling between 423 K and 673 K was applied at the hot side of the module while its cold side was maintained at 323 K. After 400 cycles (~100 hours) of testing, serious cracks occurred at the hot-side material interface, as shown in Figure 1.11b. In another example, Bi_2Te_3-based thermoelectric legs were tested by quickly switching the temperature between 253 K and 419 K at one side for ~45,000 cycles, while the other side was maintained at the ambient temperature, and the results are shown in Figures 1.11c and 11d. It can be clearly seen that cracks developed at the interface between the thermoelectric leg and the electrode, which would undoubtedly cause performance degradation. In summary, whether due to thermal shock or large interface resistance, imperfections in the contact layer can have a great impact on device performance, suggesting the importance of interface research for reliable thermoelectric modules.

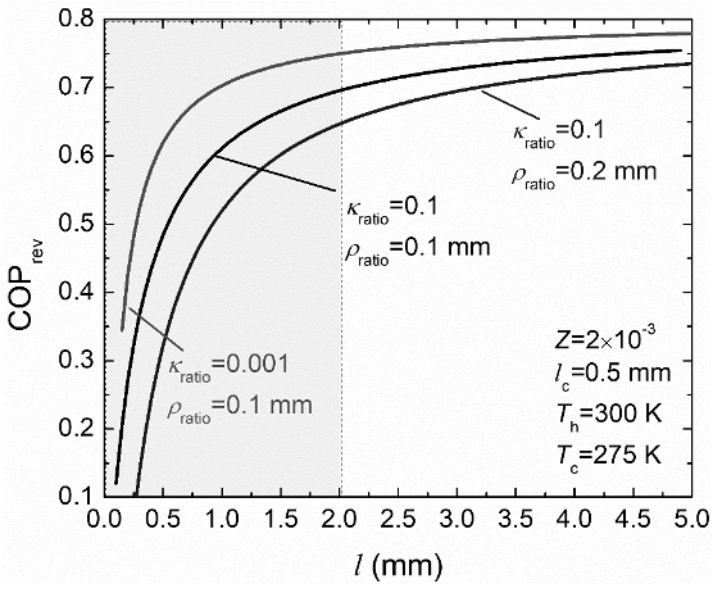

Figure 1.10. *COP_{rev} as a function of thermoelectric-leg length (l). Data obtained from Rowe (1995). For a color version of this figure, see www.iste.co.uk/akinaga/thermoelectric2.zip*

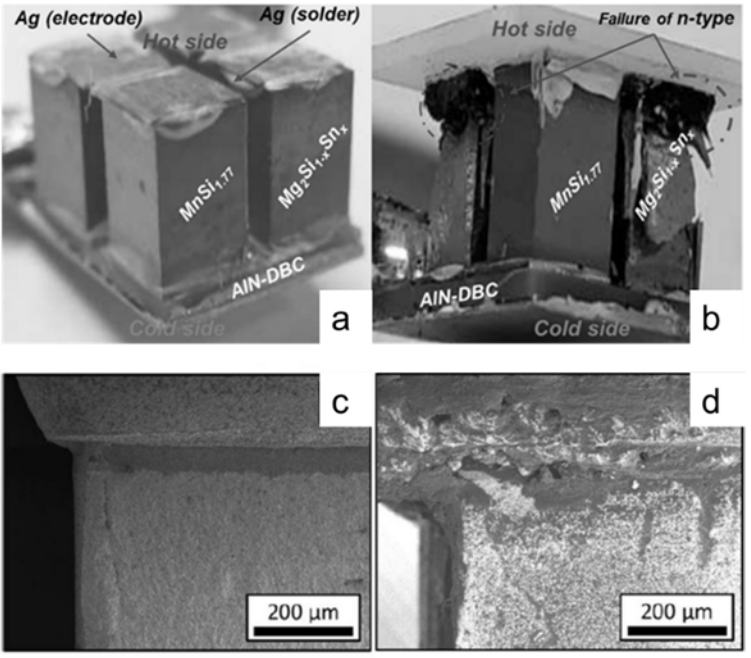

Figure 1.11. *$MnSi_{1.77}$/$Mg_2Si_{1-x}Sn_x$-based thermoelectric generator (a) before and (b) after thermal cycling between 423 K and 673 K for 100 h. Reprinted from Mejri et al. (2020). Comparison of the interface between a Cu electrode and a Bi_2Te_3 leg (c) before and (d) after thermal cycling between 253 K and 419 K for ~45,000 cycles. Reprinted from Barako et al. (2012). For a color version of this figure, see www.iste.co.uk/akinaga/thermoelectric2.zip*

1.9.2.2. *Interface design principles*

A thermoelectric device can be reduced to its essential component, a complete circuit consisting of p- and n-type thermoelectric legs (i.e. a unicouple), as schematically illustrated in Figure 1.12. The contact interface of a unicouple is a complicated region containing many layers. The design of such a multi-layer interface usually requires a more complex processing technique. Ideally, the interface design should be as simple as possible since, in practical applications, a simple interface structure facilitates manufacturing and processing. Therefore, in early studies on thermoelectric devices, researchers attempted to connect the thermoelectric legs directly to a conductive-strip (e.g. Cu) substrate. However, numerous experimental

results showed that the loss of thermoelectric energy conversion efficiency could be as high as 40% due to the large contact resistance caused by the diffusion between the bonding material and the thermoelectric legs (Ren et al. 2018). Additionally, this diffusion phenomenon also leads to performance deterioration in the thermoelectric legs, thereby shortening the service life of the device. Taking the Bi_2Te_3-based thermoelectric cooling devices as a typical case, it was found that although the Bi_2Te_3 legs and Cu strips can be joined at 503 K by using a Sn–Sb–Bi solder, the diffusion of Sn into the thermoelectric legs leads to high electrical resistance. Although the electrical resistance was reduced in later studies by replacing the Sn–Sb–Bi solder with a Sb–Ag solder, it was found that Ag diffusion into the thermoelectric legs could also be detrimental to the device (Rosi et al. 1962). In addition, Cu is also highly diffusible into Bi_2Te_3 at the operating temperature of ~523 K (Yang et al. 2013). Thus, the concept of adding a metal contact layer to serve as both the electrode and the solder diffusion barrier was proposed. For example, a Ni-metalized layer applied in a Bi_2Te_3-based thermoelectric device can effectively prevent the diffusion of the Sn from the Sn–Sb–Bi solder into the thermoelectric legs (Lin et al. 2017).

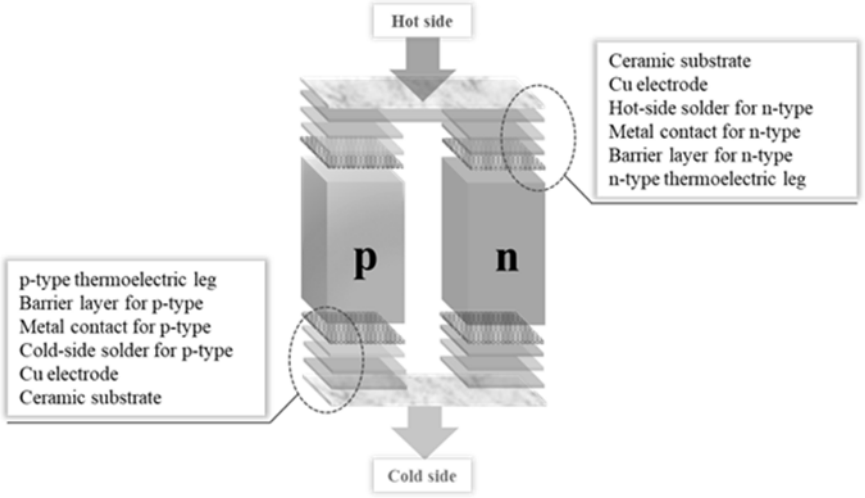

Figure 1.12. *Schematic diagram of the structure design of a thermoelectric unicouple. For a color version of this figure, see www.iste.co.uk/akinaga/thermoelectric2.zip*

A good metal contact layer and the corresponding connection technology should have the following characteristics for either a thermoelectric power generator or a thermoelectric cooler (He et al. 2018; Liu and Bai 2019): (1) the coefficient of thermal expansion (CTE) of the metal contact layer must match that of the thermoelectric leg; (2) the metalized layer must have high thermal conductivity and electrical conductivity to reduce extra energy loss at the interface; (3) low contact resistivity at the interface between the metal contact layer and the thermoelectric legs is necessary; (4) the connection technology between the metal electrodes and the thermoelectric legs should be simple, and the bonding strength should be high enough to ensure the stability of the device while operating at high temperatures and (5) avoiding doping or alloying effects due to high-temperature atomic diffusion at the interfaces is important since these could significantly alter the compositions of the thermoelectric legs and the electrode materials, leading to performance deterioration. The metal electrode should be inert to the thermoelectric material to avoid serious chemical reactions. Although diffusion is necessary for establishing a strong bond, it should be terminated when the joining is complete. In fact, it is very difficult to meet all of the above criteria at the same time. Therefore, determining how to balance various influencing factors in interface design is an important subject that needs to be studied for the development of thermoelectric devices. In general, the interface design needs to be adjusted according to actual application requirements.

From the perspective of a practical application, CTE matching is the most important issue when selecting the metal contact material since the mismatch of CTEs could cause severe internal stress, resulting in the failure of the device. Mismatched CTEs could also increase the difficulty in manufacturing thermoelectric devices. Ravi et al. (2009) carried out detailed measurements and analysis of the CTEs of some advanced thermoelectric materials, and their results confirmed that the CTE has a profound effect on the thermomechanical robustness of the devices in which these materials are incorporated. Therefore, CTE matching requires careful engineering to meet performance expectations such as long-term durability. The CTEs of various thermoelectric materials are quite different from one another, so the metal electrode materials require targeted optimization such as composition tuning in the contact layer that is sensitive to the elemental ratio of the thermoelectric legs (Liu and Bai 2019). Additionally, multi-layer

contact materials can be applied to gradually match the CTE of the thermoelectric materials.

In addition to CTE matching, a strong bond between the metal contact layer and the thermoelectric legs is essential for device reliability and durability. Generally, the metal contact layer can be made through either a chemical route (i.e. electrochemical plating or electrochemical deposition) or a physical route (i.e. sputtering, spraying, or direct hot pressing) (Zhang et al. 2016). An interface made by electrochemical plating or electrochemical deposition is very thin, and although this reduces the total electrical and thermal resistance at the contact region, the bonding strength is relatively low (~10 MPa) (Weitzaman 1967; Feng et al. 2013). This bonding strength could be adequate for refrigeration applications like commercial Bi_2Te_3-based devices, but it is far lower than that needed for power generation under thousands of thermal cycles and thermal shocks. Many studies have confirmed that increasing the surface roughness through chemical etching or sandblasting could effectively enhance the bonding strength because it would result in a larger contact surface area and an enhanced anchor point effect (Zhang 2018; Liu and Bai 2019). Compared to the chemical methods for metal contact layer production, some physical techniques produce a stronger bond between a metal electrode and the thermoelectric legs; these include thermal spraying (e.g. 18 MPa~25 MPa bonding strength between a Ni-metalized layer and a Bi_2Te_3 thermoelectric leg) (Zhang et al. 2014) and direct hot pressing (e.g. 50 MPa bonding strength between a Ti-metalized layer and a half-Heusler thermoelectric leg) (Joshi and Poudel 2016). Unfortunately, greater bonding strength is accompanied by higher contact resistance since it is usually achieved by deep interdiffusion or interface reactions in which an intermetallic layer could be formed between the metal contact layer and the thermoelectric leg. Although moderate diffusion is beneficial to interface bonding strength, uncontrolled diffusion and chemical reactions may cause increased thermal and electrical resistance, as well as significant changes in the composition of the metal contact layer and the thermoelectric legs, which will eventually cause performance deterioration in the device, or even device failure. Therefore, a balance should be found between bonding strength and other factors such as diffusion rate and contact resistance.

Using a single-layer metal contact can simplify the production process, but it makes meeting all of the above requirements at the same time difficult in some cases. For instance, there may be a large mismatch between the CTEs of the metal electrode and the thermoelectric legs; the metal contact layer could react with the thermoelectric legs quickly to form an intermetallic layer, which may lead to the deterioration of the entire device; or it may not be possible to produce a strong bond between the metal contact layer and the thermoelectric leg. Therefore, multi-layer interface technology has been introduced (Xia et al. 2014; Zhang et al. 2016; Xing et al. 2021), in which a barrier layer (also known as a transition layer) between the electrode and the thermoelectric leg serves as a buffer not only to slow down the diffusion behavior but also to improve the wettability of the material in order to facilitate brazing. Meanwhile, the barrier layer itself should also have high thermal and electrical conductivity to reduce the extra energy loss at the interface and thus improve the reliability of the device.

1.9.2.3. *Joining*

Joining processes are of great significance for the interface properties of thermoelectric modules. In particular, a proper joining technology can reduce the interface stress and improve the bonding strength, thereby increasing the reliability of the thermoelectric device to a certain extent. Over the past decades, several methods, such as the chemical and physical routes mentioned above, have been applied to join metal electrodes and thermoelectric legs. Among these methods, two major ones stand out as the most reliable and suitable for industrial manufacturing: diffusion welding and thermal spraying (see Figure 1.13). Diffusion welding, also known as one-step sintering, has been successfully applied in the fabrication of $Mg_3Sb(Bi)_2$ Zintls, MgAgSb, skutterudites, half-Heuslers, etc. (Zhao et al. 2012; Joshi and Poudel 2016; Zhang et al. 2016; Yin et al. 2020; Ying et al. 2021). As shown in Figure 1.13a, for the diffusion welding process, the electrode material powder and the thermoelectric material powder (sometimes including barrier material powder) are added into a graphite die in order, and the die is subsequently heated by using a direct hot press or a spark plasma sintering method. Using this process, the sandwich structure composed of the electrode material, barrier material and thermoelectric material powder is thus formed at one time. The main advantages of this method include its simplicity and the resulting high interface bonding strength. Thermal spraying, a newer technology, is more efficient and

scalable as compared to diffusion welding. As shown in Figure 1.13b, for the thermal spraying process, the thermoelectric material is cut to the desired dimensions for the thermoelectric legs and then plugged into a prefabricated frame made of a polymer or a ceramic. The metal electrode material and the barrier layer material can then be directly sprayed onto the contact surfaces of the thermoelectric legs. Thermal spraying is conducive to the simultaneous realization of interface processing and module integration for the device. Additionally, joins prepared by this method show higher stability at high temperatures (Zhang et al. 2016).

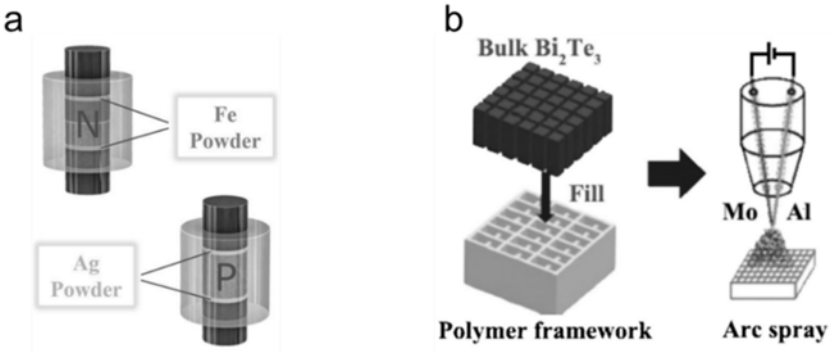

Figure 1.13. *Schematic diagrams of two major technologies for joining thermoelectric legs and metal contact layers: (a) diffusion welding. Reprinted from Ying et al. (2021) and (b) thermal spraying. Reprinted from Zhang et al. (2016). For a color version of this figure, see www.iste.co.uk/akinaga/thermoelectric2.zip*

After the metal electrode layer and the barrier layer are successfully connected to the thermoelectric legs, this working structure needs to be connected to the base (i.e. the substrate and the Cu conductive strips, which are generally joined in advance) by soldering or brazing. The selections of solder, interface pretreatment and soldering method are critical since the solder exhibits the highest CTE and the lowest yield strength among the interface components. The solder, in the form of a powder, paste or foil, is placed at the interface between the working structure and the base and should be heated and pressed to promote melting, and it is then cooled to firmly join the two parts (Kähler et al. 2014; Tewolde et al. 2015). Based on the above, one basic requirement for the solder is that its melting point should be lower than that of the thermoelectric legs and the conductive

strips. Given that the maximum stress level is located on the thermoelectric legs near the hot-side plate, the use of a low-yield soldering alloy at the hot side and the promotion of plastic deformation in the solder can result in considerable thermal stress relief. The melting point of the solder should also be higher than the operating temperature to prevent interface softening or failure of the module during service. Additionally, soldering thickness has an impact on the temperature gradient and thermal stress distribution. An optimal soldering thickness will achieve both high conversion efficiency and low thermal stress (Wu et al. 2014). Currently, the most used solder materials are Sn-based alloys, such as Sn–Ag, Sn–Cu and Au–Sn.

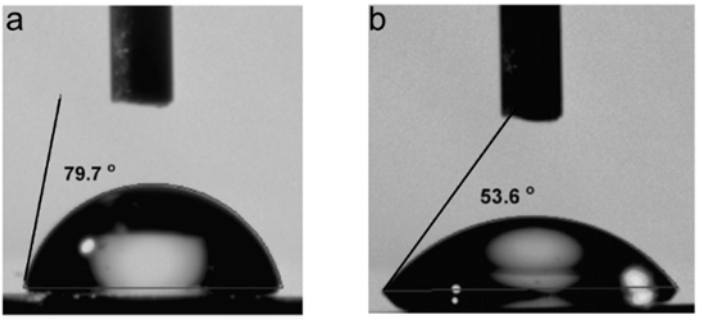

Figure 1.14. *Contact angle of a water drop on the surface of a nanostructured $Bi_2Te_{3-y}Se_y$ thermoelectric alloy (a) before and (b) after post-CMP (chemical mechanical polishing) cleaning (reprinted from Feng et al. (2011))*

It is worth noting that the quality of the soldering interface is not only associated with the type of solder and the soldering process but also with the cleanness of the interface. Careful surface cleaning is beneficial for removing surface oxides and hence reducing the contact resistance. In addition, surface cleaning can increase wettability significantly, which is beneficial for promoting welding. In a typical example, the contact angle of water dripped onto a Bi_2Te_3 surface was reduced from 79.7° to 53.6° (i.e. hydrophilicity increases) after a five-step treatment combining chemical and physical methods, as shown in Figure 1.14 (Feng et al. 2011). An interface incorporating solder has an inevitable shortcoming since it is easy to introduce contamination during the soldering process and form undesired phases which are harmful to the thermoelectric legs. In addition to applying

a metal contact layer and a barrier layer, which can reduce the deterioration on the thermoelectric legs caused by solder to a certain extent, some new joining processes, such as non-soldering-based joining, have been developed and investigated (Malik et al. 2017). The solder composition could also be adjusted appropriately for different thermoelectric compositions.

1.10. Advanced thermoelectric module case studies

In the previous section, an overview of thermoelectric device design and the major related issues was provided. Generally, the design principles described above can be applied to most thermoelectric materials. However, for particular materials, targeted strategies are required to address issues such as thermal expansion, thermal stress, bonding strength, contact resistance and interfacial reaction or diffusion due to the differences in these materials' unique characteristics and specific operating temperature ranges. Hence, the reliability-related issues of some advanced thermoelectric modules and the corresponding strategies to address these issues are introduced in the following section.

1.10.1. Bi_2Te_3

Since they are among the most successful commercial thermoelectric materials, Bi_2Te_3-based materials have been studied extensively for decades. Usually, Ni is applied as a metal contact layer (3~10 μm in thickness) in Bi_2Te_3-based devices and the diffusion of Ni at the interface is negligible when the operating temperature is under 473 K. Additionally, Ni can effectively inhibit the formation of brittle Sn–Te intermetallic compounds resulting from the reaction between Sn-containing solder and the thermoelectric matrix. Therefore, as a metal contact layer, Ni is appropriate for refrigeration applications. However, when it is applied to thermoelectric power generators, a number of problems appear. Park et al. (2012) carried out a thermal cycling test from 303 K to 433 K on a commercial Bi_2Te_3 module, as shown in Figure 1.15a. During the first 2,000 cycles, the power output was found to remain consistent with the prediction value, but between 2,000 and 6,000 cycles, there were 11% and 12% reductions in the power output for load resistance values of 47 Ω and 1,000 Ω, respectively, as shown in Figure 1.15b.

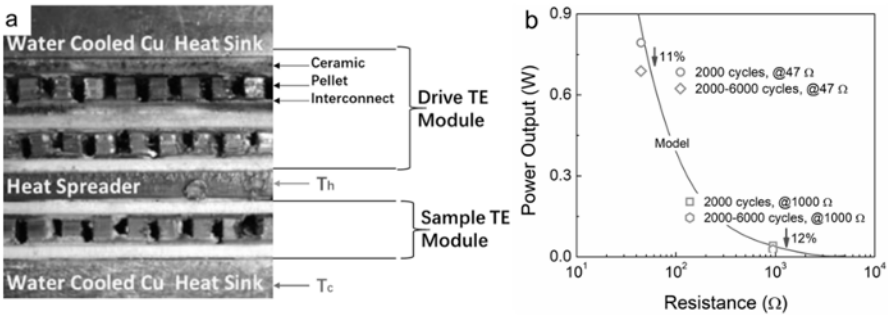

Figure 1.15. *(a) Thermal cycling test system configuration for a commercial Bi_2Te_3 module. Reprinted from Park et al. (2012). (b) Power output as a function of load resistance. Two power output data point (maximum and minimum values) for each load resistance value indicate the degradation of the thermoelectric module during thermal cycling. Data obtained from Park et al. (2012). For a color version of this figure, see www.iste.co.uk/akinaga/thermoelectric2.zip*

Liu et al. (2013) studied the interface reaction between Ni and n-type $Bi_2Te_{2.7}Se_{0.3}$ and that between Ni and p-type $Bi_{0.4}Sb_{1.6}Te_3$ by analyzing the interface microstructure of each sample hot-pressed at different temperatures, as shown in Figure 1.16. It is clear that the thickness of the interface reaction layer increases with increasing hot-pressing temperature. The thick diffusion layer is beneficial for strong bonding at the interface, but the diffusion of Ni was found to form a p-type region within the n-type $Bi_2Te_{2.7}Se_{0.3}$ leg, resulting in a large contact resistance for the n-type interface (~210 $\mu\Omega$ cm^2), while the contact resistance remains low for the p-type $Bi_{0.4}Sb_{1.6}Te_3$ leg (<1 $\mu\Omega$ cm^2) (Liu et al. 2013). Applying a barrier layer between the Ni contact layer and these thermoelectric materials is advised to address severe interface reactions at high temperatures. Additionally, seeking out new materials for the metal contact layer could be an alternative for this interface design. Research on devices based on Bi_2Te_3 remains ongoing and is currently mainly focused on improving output performance. For instance, Nozariasbmarz et al. (2020) reported that a record 8% conversion efficiency and 2.1 W/cm^2 power density were obtained in an n-/p-type Bi_2Te_3-based module for waste heat recovery (298 K~523 K). In addition, a Bi_2Te_3/half-Heusler-based segmented unicouple and a Bi_2Te_3/skutterudite segmented module also show remarkable energy

conversion efficiency around 12% (Li et al. 2020d). Unfortunately, results from aging tests and long-term service tests were not provided in these reports.

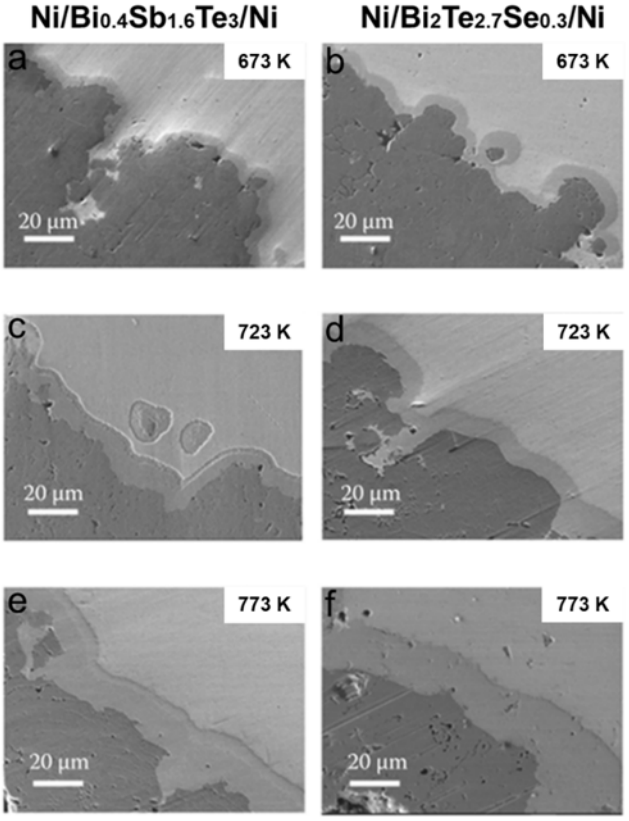

Figure 1.16. *Microstructures of contact interfaces made by directly hot-pressing Ni powder together with p-type $Bi_{0.4}Sb_{1.6}Te_3$ or n-type $Bi_2Te_{2.7}Se_{0.3}$ thermoelectric powder. Ni/$Bi_{0.4}Sb_{1.6}Te_3$/Ni hot-pressed at (a) 673 K, (c) 723 K and (e) 773 K. Ni/$Bi_2Te_{2.7}Se_{0.3}$/Ni hot-pressed at (b) 673 K, (d) 723 K and (f) 773 K. In each image, the dark region is nickel and the bright region is the thermoelectric material. Reprinted from Liu et al. (2013)*

1.10.2. *$Mg_3(Sb, Bi)_2$*

N-type $Mg_3(Sb, Bi)_2$-based materials have attracted tremendous attention in recent years because of their promising thermoelectric performance, low

cost and good mechanical properties. It is worth mentioning that $Mg_3(Sb, Bi)_2$-based devices can be used for different applications in several temperature ranges, for example, room-temperature thermoelectric cooling (Mao et al. 2019a; Shu et al. 2019a), low-grade heat recovery (Imasato et al. 2019b; Liang et al. 2021) and power generation in the medium-temperature range (Xu et al. 2021), by tuning the ratio of Sb and Bi to either Sb- or Bi-rich. As an emerging material system, $Mg_3(Sb, Bi)_2$-based thermoelectrics have received little attention in terms of interface research. Zhu et al. (2019) were the first to report on the $Mg_3(Sb, Bi)_2$ contact interface in 2019. In their study, a good junction interface with low contact resistivity and strong bonding strength was formed between $Mg_{3.1}Co_{0.1}Sb_{1.5}Bi_{0.49}Te_{0.01}$ and Fe using a direct hot-pressing method, which was found to lead to a high energy conversion efficiency of 10.6% between 373 K and 773 K. Fe has since been successfully used as a metal contact electrode layer in a thermoelectric cooling system (Mao et al. 2019a) and a low-grade waste heat recovery device (Liang et al. 2021). In a later study, Ni was found to play a role similar to that of Fe as a contact layer (Mao et al. 2019a). Ni can also ensure a low electrical contact resistance for soldering once it is electroplated on both sides of the $Mg_3(Sb, Bi)_2$ thermoelectric leg (Shang et al. 2020b; Xu et al. 2021). On the other hand, the Fe contact layer could degrade upon long-term aging, which may be attributed to the mismatched CTE values and the undesirable interface reaction between the thermoelectric material and Fe. Thus, 304 stainless steel was introduced as a potential replacement by Yin et al. (2020). An interface constructed using 304 stainless steel and a $Mg_3(Sb, Bi)_2$-based thermoelectric material shows smaller changes in its electrical and mechanical properties with aging compared to that constructed using Fe due to its suppressed diffusion and enhanced expansion coefficient match, as shown in Figure 1.17. A high conversion efficiency of up to 9% at a temperature difference of 370 K in a single leg incorporating this $Mg_3(Sb, Bi)_2$-based thermoelectric material and 304 stainless steel was reported in the same study. Unfortunately, no studies of the long-term operation of an integrated module based on $Mg_3(Sb, Bi)_2$ have yet been reported. In short, despite the good thermoelectric properties of $Mg_3(Sb, Bi)_2$-based materials, only with abundant contact layer research and module evaluation can these compounds achieve a large-scale practical application.

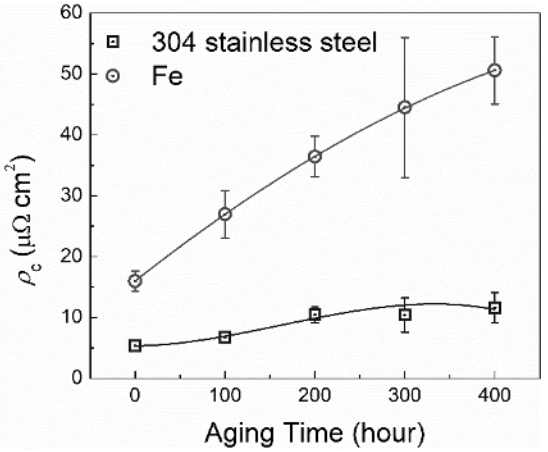

Figure 1.17. *Aging-time-dependent contact resistivity of $Mg_{3.2}Sb_{1.5}Bi_{0.49}Te_{0.01}$/304 stainless steel and $Mg_{3.2}Sb_{1.5}Bi_{0.49}Te_{0.01}$/Fe junctions aged at 523 K. Data obtained from Yin et al. (2020). For a color version of this figure, see www.iste.co.uk/akinaga/thermoelectric2.zip*

1.10.3. *GeTe*

Research on GeTe as a thermoelectric material began as early as the 1960s, but it was not studied in depth for long since it has an excessively high carrier concentration (~10^{21} cm^{-3}) and an undesired phase change at ~700 K. In recent years, GeTe has returned as a focus of thermoelectric research because it was found that its carrier concentration can be reduced to an ideal range (~10^{20} cm^{-3}) by doping with Sb or Bi (Liu et al. 2018; Zheng et al. 2018). Additionally, its undesired phase transition can be suppressed by element doping, as discussed in section 1.5. GeTe has subsequently become a promising candidate for use in thermoelectric generators for waste heat recovery in the mid-temperature range. Although the thermoelectric performance of GeTe has been greatly improved, device research is currently lagging significantly, delaying actual applications. At high temperatures, fast chemical reactions and diffusion can occur between the metal electrodes and the thermoelectric legs in GeTe-based thermoelectric modules. Thus, a barrier layer is required. An Al–Si alloy was recently proposed as a diffusion barrier for GeTe-based thermoelectric legs by Li et al. (2020b). In their study, a good connection between $Al_{66}Si_{34}$ and $Ge_{0.9}Sb_{0.1}TeB_{0.01}$ was obtained using the spark plasma sintering method and the resulting thermoelectric legs underwent aging testing for 16 days at 773 K. After the

16-day test, their contact resistivity increased slightly from 20.7 to 26.1 $\mu\Omega\cdot cm^2$. The thickness of the interface diffusion layer increased quickly from ~8 to ~18 μm during the first 4 days of aging but slowed down after 8 days of aging. Overall, the thickness of the interface diffusion layer increased to ~23 μm after 16 days of aging, as shown in Figure 1.18a–c. The shear strength of the thermoelectric legs also increased from 26.6 MPa to 41.7 MPa after the aging test, which may be attributed to the thicker diffusion layer. Xing et al. (2021) chose Mo as an effective diffusion barrier material for GeTe-based thermoelectric legs by testing 12 pure metals (Cr, Hf, Nb, Ti, Mo, Ni, Ta, Zr, Al, Co, V and Fe). The result of resistance line scanning across the interface of GeTe/Mo/GeTe indicates that an extraordinarily low value (less than 1 $\mu\Omega\cdot cm^2$) can be obtained. Furthermore, a $Ge_{0.92}Sb_{0.04}Bi_{0.04}Te_{0.95}Se_{0.05}$/Mo/Ni thermoelectric leg was constructed and underwent aging testing at 800 K, and its interface microstructure was found to remain stable after 10 days of testing, as shown in Figure 1.18d–f. Finally, an eight-couple $Ge_{0.92}Sb_{0.04}Bi_{0.04}Te_{0.95}Se_{0.05}/Yb_{0.3}Co_4Sb_{12}$ thermoelectric module was fabricated and achieved an energy conversion efficiency of 7.8% and a power density of 1.1 $W\cdot cm^{-2}$ under a temperature difference of 500 K.

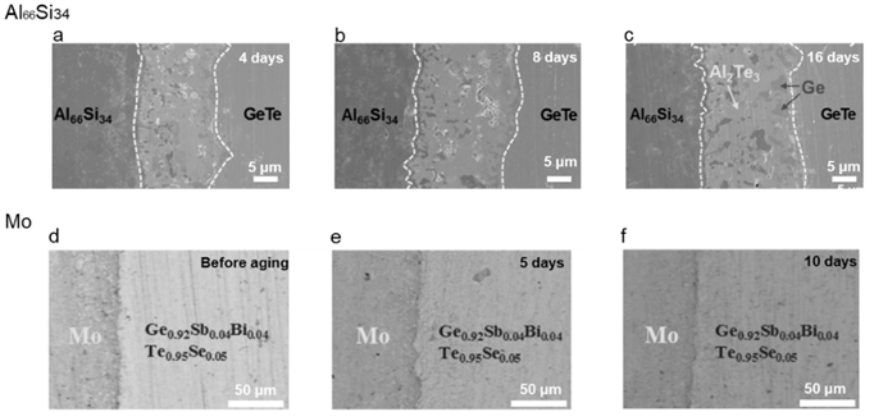

Figure 1.18. *Scanning electron microscopy images of the interface area of $Ge_{0.9}Sb_{0.1}TeB_{0.01}/Al_{66}Si_{34}$ thermoelectric legs after (a) 4 days, (b) 8 days and (c) 16 days of aging at 773 K. Reprinted from Li et al. (2020b). Scanning electron microscopy images of the interface area of $Ge_{0.92}Sb_{0.04}Bi_{0.04}Te_{0.95}Se_{0.05}$/Mo/Ni thermoelectric legs (d) before aging and after aging (e) 5 days and (f) 10 days at 800 K. Reprinted from Xing et al. (2021). For a color version of this figure, see www.iste.co.uk/akinaga/thermoelectric2.zip*

1.10.4. *Skutterudites*

Filled skutterudites show promising thermoelectric and mechanical properties for mid-temperature power generation. The contact design of skutterudites has been extensively examined in recent decades. Pure metals and alloys like Ni, Ti, Zr, Nb, Mo-Cu and Co-Fe-Ni have been employed and evaluated as metal contact layers (Zhang 2018; Liu and Bai 2019). Although Ni is a good candidate for most thermoelectric materials in interfacial design, it is not suitable for skutterudites due to its larger CTE. Therefore, a buffer layer is needed when Ni is applied as the metal contact layer for skutterudites. Ti- and Zr-based contact layers often suffer from a severe interfacial chemical reaction during the aging process, so they do not provide adequate stability for long-term power generation service. The Mo–Cu alloy is another potential candidate for the metal contact layer because of its high electrical and thermal conductivity. Additionally, its composition can be easily tuned to match the CTE of the filled skutterudite (Zhang 2018). However, it is very difficult to bond the Mo–Cu alloy onto the surface of a skutterudite thermoelectric leg. In fact, the most significant challenge in choosing a metal contact layer for skutterudites is that their main element, Sb, is highly reactive, which may cause a severe interfacial reaction and diffusion at high temperatures, and thus significantly degrade the device performance. To balance effective bonding and a durable interface, Chu et al. (2020) recently proposed a criterion to predict the bonding behavior as well as the interfacial reliability of $CoSb_3$-based filled skutterudite/metal electrode interfaces by combining the interfacial reaction energy (E_{IR}) value of a metal with its Sb migration activation energy barrier (E_{Mig}) value, as shown in Figure 1.19a. Generally, E_{IR} should be negative to promote the progress of the interface reaction and produce a mechanical force at the interface, while E_{Mig} should be large enough to limit Sb diffusion and prevent the interface reaction layer from growing too quickly. Based on their simulation results, they defined a “sweet spot” area as shown in Figure 1.19a, and metals in this region were determined to be potential candidates for the metal contact layer. To validate the proposed criterion, Nb was chosen as the metal contact layer to fabricate a $CoSb_3$-based filled skutterudite thermoelectric leg. Their experimental results showed robust bonding with no obvious diffusion under thermal cycles, confirming that the interface reaction was inhibited and the interfacial resistivity was reduced. The derived module also showed excellent stability in output power as well as internal resistance after 846 hours of service testing, as shown in Figure 1.19b. In addition, work–function matching is another effective guiding principle for interfacial design that was proposed by Jie et al. (2015). They

reported that the matching of the work function between a metal contact layer and a filled skutterudite can play a crucial role in determining the electrical contact resistance based on their study of the interface behavior between the p-type $Ce_{0.45}Nd_{0.45}Fe_{3.5}Co_{0.5}Sb_{12}$ and a Cr–Fe–Co alloy or a Cr–Fe–Ni alloy.

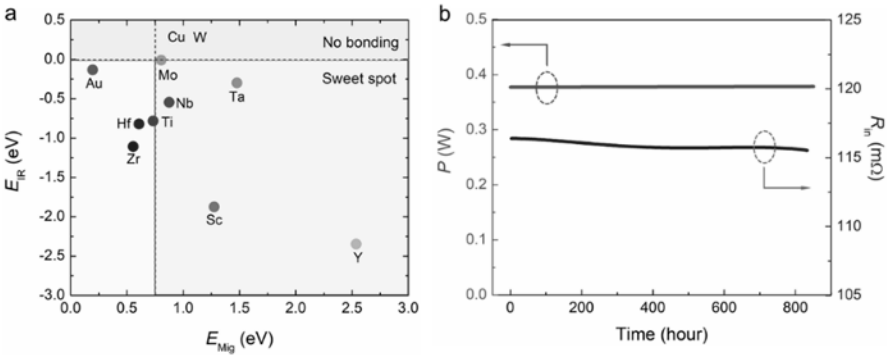

Figure 1.19. *(a) Correlation map of interfacial reaction energy (E_{IR}) and Sb migration activation energy barrier (E_{Mig}) values of different metals. (b) Output power and internal resistance of an eight-pair $CoSb_3$-based filled skutterudite module fabricated using Nb as the barrier layer under long-term service conditions with T_h = 818 K and T_c = 308 K. Data obtained from Chu et al. (2020). For a color version of this figure, see www.iste.co.uk/akinaga/thermoelectric2.zip*

1.11. Summary and outlook

In comparison with zT improvement among various thermoelectric materials over the past decades, the development process from thermoelectric materials to devices has been much slower. For the materials' optimization, more effort should be devoted to improving the thermal stability and mechanical robustness of the materials with relatively high zT because commercialization will not be possible until such improvement is achieved. To accelerate commercialization, a multi-criteria evaluation method needs to be developed based on the performance and reliability requirements. Since the interfacial layer plays an important role in performance maximization and structure integrity, it is meaningful to construct a rational model based on experiment and simulation to guide the design of high-performance contact layers. For device development, evaluating the performance of each lab-prepared module based on multiple industrial standards (e.g. vibration testing, mechanical shock testing,

temperature cycle endurance testing, etc.) can help to determine commercial viability in realizing actual applications. Most importantly, it is time to try all possible device applications to demonstrate some of the promise of the past decades of materials research to build a case for economical adaption of this technology to real applications. With enough practical applications of thermoelectric devices, more research will be funded and can be carried out, which in turn will enhance the device applications. Such a healthy, self-propelling cycle is what the thermoelectric research community needs going forward.

1.12. References

Al-Merbati, A.S., Yilbas, B.S., Sahin, A.Z. (2013). Thermodynamics and thermal stress analysis of thermoelectric power generator: Influence of pin geometry on device performance. *Appl. Therm. Eng*., 50(1), 683–692.

Barako, M.T., Park, W., Marconnet, A.M., Asheghi, M., Goodson, K.E. (2012). Thermal cycling, mechanical degradation, and the effective figure of merit of a thermoelectric module. *J. Electron. Mater.*, 42(3), 372–381.

Bohra, A.K., Bhatt, R., Bhattacharya, S., Basu, R., Ahmad, S., Singh, A., Aswal, D.K., Gupta, S.K. (2016). Study of thermal stability of Cu_2Se thermoelectric material. *AIP Conf. Proc.*, 1713, 110010.

Bohra, A.K., Bhatt, R., Singh, A., Bhattacharya, S., Basu, R., Bhatt, P., Navaneethan, M., Sarkar, S.K., Anwar, S., Muthe, K.P. et al. (2020). Stabilizing thermoelectric figure-of-merit of superionic conductor Cu_2Se through nanoinclusions. *Phys. Status Solidi (RRL)*, 14, 2000102.

Chen, L.D., Dong, H.L., Li, X.Y., Huang, X.Y., Jiang, W., Tang, Y.S., Xia, X.G., Liao, J.C., He, L. (2013). Skutterudite based thermoelectric material, thermal protection coating for devices and preparation method thereof. Patent, CN103146301A.

Chowdhury, I., Prasher, R., Lofgreen, K., Chrysler, G., Narasimhan, S., Mahajan, R., Koester, D., Alley, R., Venkatasubramanian, R. (2009). On-chip cooling by superlattice-based thin-film thermoelectrics. *Nat. Nanotechnol.*, 4(4), 235–238.

Chu, J., Huang, J., Liu, R., Liao, J., Xia, X., Zhang, Q., Wang, C., Gu, M., Bai, S., Shi, X. et al. (2020). Electrode interface optimization advances conversion efficiency and stability of thermoelectric devices. *Nat. Commun.*, 11(1), 2723.

Dasgupta, T., Stiewe, C., Sesselmann, A., Yin, H., Iversen, B.B., Mueller, E. (2013). Thermoelectric studies in β-Zn_4Sb_3-the complex interdependence between thermal stability, thermoelectric transport, and zinc content. *J. Appl. Phys.*, 113, 103708.

Deng, S., Chen, Z., Li, D., Liu, H., Tang, Y., Shen, L., Deng, S. (2017). Effect of Pb doped on thermal stability and electrical transport properties of single crystalline β-Zn_4Sb_3. *Physica B*, 526, 155–159.

Dong, H., Li, X., Tang, Y., Zou, J., Huang, X., Zhou, Y., Jiang, W., Zhang, G.-J., Chen, L. (2012). Fabrication and thermal aging behavior of skutterudites with silica-based composite protective coatings. *J. Alloys Compd.*, 527, 247–251.

El-Genk, M.S., Saber, H.H., Caillat, T., Sakamoto, J. (2006). Tests results and performance comparisons of coated and un-coated skutterudite based segmented unicouples. *Energy Convers. Manag.*, 47(2), 174–200.

Erturun, U., Erermis, K., Mossi, K. (2015). Influence of leg sizing and spacing on power generation and thermal stresses of thermoelectric devices. *Appl. Energy*, 159, 19–27.

Fabián-Mijangos, A., Min, G., Alvarez-Quintana, J. (2017). Enhanced performance thermoelectric module having asymmetrical legs. *Energy Convers. Manag.*, 148, 1372–1381.

Feng, H.-P., Yu, B., Chen, S., Collins, K., He, C., Ren, Z.F., Chen, G. (2011). Studies on surface preparation and smoothness of nanostructured Bi_2Te_3-based alloys by electrochemical and mechanical methods. *Electrochim. Acta*, 56(8), 3079–3084.

Feng, S.P., Chang, Y.H., Yang, J., Poudel, B., Yu, B., Ren, Z., Chen, G. (2013). Reliable contact fabrication on nanostructured Bi_2Te_3-based thermoelectric materials. *Phys. Chem. Chem. Phys.*, 15(18), 6757–6762.

Hao, Y., Pedersen, B.L., Iversen, B.B. (2011). Thermal stability of high performance thermoelectric β-Zn_4Sb_3 in argon. *Eur. J. Inorg. Chem.*, 17, 2733–2737.

He, R., Schierning, G., Nielsch, K. (2018). Thermoelectric devices: A review of devices, architectures, and contact optimization. *Adv. Mater. Technol.*, 3(4), 1700256.

Hong, M., Zheng, K., Lyv, W., Li, M., Qu, X., Sun, Q., Xu, S., Zou, J., Chen, Z.-G. (2020). Computer-aided design of high-efficiency GeTe-based thermoelectric devices. *Energy Environ. Sci.*, 13(6), 1856–1864.

Imasato, K., Wood, M., Kuo, J.J., Snyder, G.J. (2018). Improved stability and high thermoelectric performance through cation site doping in n-type La-doped $Mg_3Sb_{1.5}Bi_{0.5}$. *J. Mater. Chem. A*, 6(41), 19941–19946.

Imasato, K., Kang, S.D., Snyder, G.J. (2019). Exceptional thermoelectric performance in $Mg_3Sb_{0.6}Bi_{1.4}$ for low-grade waste heat recovery. *Energy Environ. Sci.*, 12, 965–971.

Ioffe, A.F. (1957). *Semiconductor Thermoelements and Thermoelectric Cooling*. Infosearch Ltd, London.

Jia, X. and Gao, Y. (2014). Estimation of thermoelectric and mechanical performances of segmented thermoelectric generators under optimal operating conditions. *Appl. Therm. Eng.*, 73(1), 335–342.

Jie, Q., Ren, Z., Chen, G. (2015). Fabrication of stable electrode/diffusion barrier layers for thermoelectric filled skutterudite devices. Patent, US9722164B2.

Jørgensen, L.R., Zhang, J., Zeuthen, C.B., Iversen, B.B. (2018). Thermal stability of $Mg_3Sb_{1.475}Bi_{0.475}Te_{0.05}$ high performance n-type thermoelectric investigated through powder X-ray diffraction and pair distribution function analysis. *J. Mater. Chem. A*, 6(35), 17171–17176.

Joshi, G. and Poudel, B. (2016). Efficient and robust thermoelectric power generation device using hot-pressed metal contacts on nanostructured half-Heusler alloys. *J. Electron. Mater.*, 45(12), 6047–6051.

Kähler, J., Stranz, A., Waag, A., Peiner, E. (2014). Thermoelectric coolers with sintered silver interconnects. *J. Electron. Mater.*, 43(6), 2397–2404.

Kambe, M., Jinushi, T., Ishijima, Z. (2010). Encapsulated thermoelectric modules and compliant pads for advanced thermoelectric systems. *J. Electron. Mater.*, 39(9), 1418–1421.

Kang, S.D., Pohls, J.-H., Aydemir, U., Qiu, P., Stoumpos, C.C., Hanus, R., White, M.A., Shi, X., Chen, L., Kanatzidis, M.G. et al. (2017). Enhanced stability and thermoelectric figure-of-merit in copper selenide by lithium doping. *Mater. Today Phys.*, 1, 7–13.

Karri, N.K. and Mo, C. (2018). Structural reliability evaluation of thermoelectric generator modules: Influence of end conditions, leg geometry, metallization, and processing temperatures. *J. Electron. Mater.*, 47(10), 6101–6120.

Kim, C.N. (2018). Development of a numerical method for the performance analysis of thermoelectric generators with thermal and electric contact resistance. *Appl. Therm. Eng.*, 130, 408–417.

Kim, H.S., Wang, T., Liu, W., Ren, Z. (2016). Engineering thermal conductivity for balancing between reliability and performance of bulk thermoelectric generators. *Adv. Funct. Mater.*, 26(21), 3678–3686.

Kim, H.S., Liu, W., Ren, Z. (2017). The bridge between the materials and devices of thermoelectric power generators. *Energy Environ. Sci.*, 10(1), 69–85.

Kuo, J.J., Yu, Y., Kang, S.D., Cojocaru-Mirédin, O., Wuttig, M., Snyder, G.J. (2019). Mg deficiency in grain boundaries of *n*-type Mg_3Sb_2 identified by atom probe tomography. *Adv. Mater. Inter.*, 6(13), 1900429.

Li, F., Wei, T.-R., Kang, F., Li, J.-F. (2014). Thermal stability and oxidation resistance of BiCuSeO based thermoelectric ceramics. *J. Alloys Compd*., 614, 394–400.

Li, J., Jia, F., Zhang, S., Zheng, S., Wang, B., Chen, L., Lu, G., Wu, L. (2019). The manipulation of substitutional defects for realizing high thermoelectric performance in Mg_3Sb_2-based Zintl compounds. *J. Mater. Chem. A*, 7(33), 19316–19323.

Li, J., Zhang, S., Jia, F., Zheng, S., Shi, X., Jiang, D., Wang, S., Lu, G., Wu, L., Chen, Z.-G. (2020a). Point defect engineering and machinability in n-type Mg_3Sb_2-based materials. *Mater. Today Phys.*, 15, 100269.

Li, J., Zhao, S., Chen, J., Han, C., Hu, L., Liu, F., Ao, W., Li, Y., Xie, H., Zhang, C. (2020b). Al–Si alloy as a diffusion barrier for GeTe-based thermoelectric legs with high interfacial reliability and mechanical strength. *ACS Appl. Mater. Interfaces*, 12(16), 18562–18569.

Li, M., Hong, M., Tang, X., Sun, Q., Lyu, W.-Y., Xu, S.-D., Kou, L.-Z., Dargusch, M., Zou, J., Chen, Z.-G. (2020c). Crystal symmetry induced structure and bonding manipulation boosting thermoelectric performance of GeTe. *Nano Energy*, 73, 104740.

Li, W., Poudel, B., Nozariasbmarz, A., Sriramdas, R., Zhu, H., Kang, H.B., Priya, S. (2020d). Bismuth telluride/half-Heusler segmented thermoelectric unicouple modules provide 12% conversion efficiency. *Adv. Energy Mater.*, 10(38), 2001924.

Li, M., Sun, Q., Xu, S.D., Hong, M., Lyu, W.Y., Liu, J.X., Wang, Y., Dargusch, M., Zou, J., Chen, Z.G. (2021). Optimizing electronic quality factor toward high-performance $Ge_{1-x-y}Ta_xSb_yTe$ thermoelectrics: The role of transition metal doping. *Adv. Mater.*, 33(40), 2102575.

Liang, Z., Xu, C., Shang, H., Zhu, Q., Ding, F., Mao, J., Ren, Z. (2021). High thermoelectric energy conversion efficiency of a unicouple of n-type Mg_3Bi_2 and p-type Bi_2Te_3. *Mater. Today Phys.*, 19, 100413.

Lin, W.-C., Li, Y.-S., Wu, A.T. (2017). Study of diffusion barrier for solder/n-type Bi_2Te_3 and bonding strength for p- and n-type thermoelectric modules. *J. Electron. Mater.*, 47(1), 148–154.

Liu, W. and Bai, S. (2019). Thermoelectric interface materials: A perspective to the challenge of thermoelectric power generation module. *J. Mater.*, 5(3), 321–336.

Liu, H., Shi, X., Xu, F., Zhang, L., Zhang, W., Chen, L., Li, Q., Uher, C., Day, T., Snyder, G.J. (2012). Copper ion liquid-like thermoelectrics. *Nat. Mater.*, 11(5), 422–425.

Liu, W., Wang, H., Wang, L., Wang, X., Joshi, G., Chen, G., Ren, Z. (2013). Understanding of the contact of nanostructured thermoelectric n-type $Bi_2Te_{2.7}Se_{0.3}$ legs for power generation applications. *J. Mater. Chem. A*, 1, 13093–13100.

Liu, W., Jie, Q., Kim, H.S., Ren, Z. (2015). Current progress and future challenges in thermoelectric power generation: From materials to devices. *Acta Mater.*, 87, 357–376.

Liu, Z., Sun, J., Mao, J., Zhu, H., Ren, W., Zhou, J., Wang, Z., Singh, D.J., Sui, J., Chu, C.W. et al. (2018). Phase-transition temperature suppression to achieve cubic GeTe and high thermoelectric performance by Bi and Mn codoping. *Proc. Natl. Acad. Sci. USA*, 115(21), 5332–5337.

Liu, W., Shen, L., Shai, X., Tang, Y., Chen, Z., Sun, L., Ge, W., Deng, S. (2019). Effect of hole modulation on the electrical transport properties and thermal stability of single crystal α-Cu_2Se prepared by Bi-flux method. *J. Alloy. Compd.*, 791, 60–67.

Liu, Z.-Y., Zhu, J.-L., Tong, X., Niu, S., Zhao, W.-Y. (2020). A review of $CoSb_3$-based skutterudite thermoelectric materials. *J. Adv. Ceram.*, 9(6), 647–673.

Lu, J., Li, D., Liu, W., Shen, L., Chen, J., Ge, W., Deng, S. (2020a). Thermal stability and thermoelectric properties of Cd-doped nano-layered Cu_2Se prepared using NaCl flux method. *Chin. Phys. B*, 29, 127403.

Lu, R., Olvera, A., Bailey, T.P., Uher, C., Poudeu, F.P. (2020b). Nanoscale engineering of polymorphism in Cu_2Se-based composites. *ACS Appl. Mater. Interfaces*, 12(28), 31601–31611.

Malik, S.A., Hung, L.T., Van Nong, N. (2017). Solder free joining as a highly effective method for making contact between thermoelectric materials and metallic electrodes. *Mater. Today Energy*, 5, 305–311.

Mao, J., Shuai, J., Song, S., Wu, Y., Dallye, R., Zhou, J., Liu, Z., Sun, J., Zhang, Q., Cruz, C.D. et al. (2017a). Manipulation of ionized impurity scattering for achieving high thermoelectric performance in n-type Mg_3Sb_2-based materials. *Proc. Natl. Acad. Sci. USA*, 114(40), 10548–10553.

Mao, J., Wu, Y., Song, S., Zhu, Q., Shuai, J., Liu, Z., Pei, Y., Ren, Z. (2017b). Defect engineering for realizing high thermoelectric performance in n-type Mg_3Sb_2-based materials. *ACS Energy Lett.*, 2(10), 2245–2250.

Mao, J., Liu, Z., Zhou, J., Zhu, H., Zhang, Q., Chen, G., Ren, Z. (2018). Advances in thermoelectrics. *Adv. Phys.*, 67(2), 69–147.

Mao, J., Zhu, H., Ding, Z., Liu, Z., Gamage, G.A., Chen, G., Ren, Z. (2019a). High thermoelectric cooling performance of n-type Mg_3Bi_2-based materials. *Science*, 365(6452), 495–498.

Mao, T., Qiu, P., Du, X., Hu, P., Zhao, K., Xiao, J., Shi, X., Chen, L. (2019b). Enhanced thermoelectric performance and service stability of Cu_2Se via tailoring chemical compositions at multiple atomic positions. *Adv. Funct. Mater*., 30(6), 1908315.

Mejri, M., Malard, B., Thimont, Y., Romanjek, K., Ihou Mouko, H., Estournès, C. (2020). Thermal stability of $Mg_2Si_{0.55}Sn_{0.45}$ for thermoelectric applications. *J. Alloys Compd.*, 846, 156413.

Moghaddam, A.O., Shokuhfar, A., Zhang, Y., Zhang, T., Cadavid, D., Arbiol, J., Cabot, A. (2019). Ge-doped ZnSb/β-Zn_4Sb_3 nanocomposites with high thermoelectric performance. *Adv. Mater. Interfaces*, 6(18), 1900467.

Music, D., Geyer, R.W., Keuter, P. (2016). Thermomechanical response of thermoelectrics. *Appl. Phys. Lett.*, 109(22), 223903.

Ni, J.E., Case, E.D., Schmidt, R.D., Wu, C.-I., Hogan, T.P., Trejo, R.M., Kirkham, M.J., Lara-Curzio, E., Kanatzidis, M.G. (2013). The thermal expansion coefficient as a key design parameter for thermoelectric materials and its relationship to processing-dependent bloating. *J. Mater. Sci.*, 48(18), 6233–6244.

Nozariasbmarz, A., Poudel, B., Li, W., Kang, H.B., Zhu, H., Priya, S. (2020). Bismuth telluride thermoelectrics with 8% module efficiency for waste heat recovery application. *Science*, 23(7), 101340.

Nunn, R., Qiu, P., Yin, M., Chen, H., Hanus, R., Song, Q., Zhang, T., Chou, M.-Y., Agne, M.T., He, J. et al. (2017). Ultrahigh thermoelectric performance in Cu_2Se-based hybrid materials with highly dispersed molecular CNTs. *Energy Environ. Sci.*, 10, 1928–1935.

Park, W., Marconnet, A.M., Asheghi, M., Goodson, K.E. (2012). *13th InterSociety Conference on Thermal and Thermomechanical Phenomena in Electronic Systems*. IEEE, San Diego.

Rausch, E., Balke, B., Ouardi, S., Felser, C. (2016). Long-term stability of (Ti/Zr/Hf)$CoSb_{1-x}Sn_x$ thermoelectric p-type half-Heusler compounds upon thermal cycling. *Energy Technol.*, 3, 1217–1224.

Ravi, V., Firdosy, S., Caillat, T., Brandon, E., Van Der Walde, K., Maricic, L., Sayir, A. (2009). Thermal expansion studies of selected high-temperature thermoelectric materials. *J. Electron. Mater.*, 38(7), 1433–1442.

Ren, Z., Lan, Y., Zhang, Q. (2018). *Advanced Thermoelectrics: Materials, Contacts, Devices, and Systems*. CRC Press, New York.

Rogl, G. and Rogl, P. (2017). How nanoparticles can change the figure of merit, ZT, and mechanical properties of skutterudites. *Mater. Today Phys.*, 3, 48–69.

Rogl, G., Zhang, L., Rogl, P., Grytsiv, A., Falmbigl, M., Rajs, D., Kriegisch, M., Müller, H., Bauer, E., Koppensteiner, J. et al. (2010). Thermal expansion of skutterudites. *Int. J. Appl. Phys.*, 107(4), 043507.

Rosi, F.D. and Bernoff, R.A. (1962). Method and materials for obtaining low resistance bonds to thermoelectric bodies. Patent, US3037064A.

Rowe, D.M. (1995). *Thermoelectrics Handbook*. CRC Press, London.

Sakamoto, J.S., Snyder, G.J., Calliat, T., Fleurial, J.P., Jones, S.M., Palk, J.A. (2008). System and method for suppressing sublimation using opacified aerogel. Patent, US7461512B2.

Sales, B.C., Mandrus, D., Williams, R.K. (1996). Filled skutterudite antimonides: A new class of thermoelectric materials. *Science*, 272(5266), 1325–1328.

Sarhadi, A., Bjørk, R., Pryds, N. (2015). Optimization of the mechanical and electrical performance of a thermoelectric module. *J. Electron. Mater.*, 44(11), 4465–4472.

Shai, X., Deng, S., Shen, L., Meng, D., Li, D., Zhang, Y., Jiang, X. (2015). Preparation, thermal stability, and electrical transport properties of In/Sn codoped b-Zn_4Sb_3 single crystal. *Phys. Status Solidi B*, 252(4), 1–5.

Shang, H., Liang, Z., Xu, C., Mao, J., Gu, H., Ding, F., Ren, Z. (2020a). N-type $Mg_3Sb_{2-x}Bi_x$ alloys as promising thermoelectric materials. *Research*, 1219461.

Shang, H., Liang, Z., Xu, C., Song, S., Huang, D., Gu, H., Mao, J., Ren, Z., Ding, F. (2020b). N-type $Mg_3Sb_{2-x}Bi_x$ with improved thermal stability for thermoelectric power generation. *Acta Mater.*, 201, 572–579.

Shi, X., Sun, C., Bu, Z., Zhang, X., Wu, Y., Lin, S., Li, W., Faghaninia, A., Jain, A., Pei, Y. (2019a). Revelation of inherently high mobility enables Mg_3Sb_2 as a sustainable alternative to n-Bi_2Te_3 thermoelectrics. *Adv. Sci.*, 6(16), 1802286.

Shi, X., Sun, C., Zhang, X., Chen, Z., Lin, S., Li, W., Pei, Y. (2019b). Efficient Sc-doped $Mg_{3.05-x}Sc_xSbBi$ thermoelectrics near room temperature. *Chem. Mater.*, 31(21), 8987–8994.

Shi, X., Zhao, T., Zhang, X., Sun, C., Chen, Z., Lin, S., Li, W., Gu, H., Pei, Y. (2019c). Extraordinary n-type Mg_3SbBi thermoelectrics enabled by yttrium doping. *Adv. Mater.*, 31(36), 1903387.

Shi, D., Geng, Z., Shi, L., Li, Y., Lam, K.H. (2020). Thermal stability study of $Cu_{1.97}Se$ superionic thermoelectric material. *J. Mater. Chem. C*, 8, 10221–10228.

Shittu, S., Li, G., Zhao, X., Ma, X. (2020). Review of thermoelectric geometry and structure optimization for performance enhancement. *Appl. Energy*, 268(150), 115075.

Shu, R., Zhou, Y., Wang, Q., Han, Z., Zhu, Y., Liu, Y., Chen, Y., Gu, M., Xu, W., Wang, Y. et al. (2019). $Mg_{3+\delta}Sb_xBi_{2-x}$ family: A promising substitute for the state-of-the-srt n-type thermoelectric materials near room temperature. *Adv. Funct. Mater.*, 29(4), 1807235.

Shuai, J., Mao, J., Song, S., Zhang, Q., Chen, G., Ren, Z. (2017a). Recent progress and future challenges on thermoelectric Zintl materials. *Mater. Today Phys.*, 1, 74–95.

Shuai, J., Mao, J., Song, S., Zhu, Q., Sun, J., Wang, Y., He, R., Zhou, J., Chen, G., Singh, D.J. et al. (2017b). Tuning the carrier scattering mechanism to effectively improve the thermoelectric properties. *Energy Environ. Sci.*, 10(3), 799–807.

Shuai, J., Ge, B., Mao, J., Song, S., Wang, Y., Ren, Z. (2018). Significant role of Mg stoichiometry in designing high thermoelectric performance for $Mg_3(Sb,Bi)_2$-based n-type Zintls. *J. Am. Chem. Soc.*, 140(5), 1910–1915.

Shuai, J., Tan, X.J., Guo, Q., Xu, J.T., Gellé, A., Gautier, R., Halet, J.F., Failamani, F., Jiang, J., Mori, T. (2019). Enhanced thermoelectric performance through crystal field engineering in transition metal-doped GeTe. *Mater. Today Phys.*, 9, 100094.

Song, L., Blichfeld, A.B., Zhang, J., Kasai, H., Iversena, B.B. (2018). Enhanced thermoelectric performance and high-temperature thermal stability of p-type Ag-doped β-Zn_4Sb_3. *J. Mater. Chem. A*, 6, 4079–4087.

Song, S., Mao, J., Bordelon, M., He, R., Wang, Y., Shuai, J., Sun, J., Lei, X., Ren, Z., Chen, S. et al. (2019). Joint effect of magnesium and yttrium on enhancing thermoelectric properties of n-type Zintl $Mg_{3+\delta}Y_{0.02}Sb_{1.5}Bi_{0.5}$. *Mater. Today Phys.*, 8, 25–33.

Sun, W., Sui, R., Yuan, G., Zheng, H., Zeng, Z., Xie, P., Yuan, L., Ren, Z., Cai, F., Zhang, Q. (2021). Thermoelectric module design to improve lifetime and output power density. *Mater. Today Phys.*, 18, 100391.

Tamaki, H., Sato, H.K., Kanno, T. (2016). Isotropic conduction network and defect chemistry in $Mg_{3+\delta}Sb_2$-based layered Zintl compounds with high thermoelectric performance. *Adv. Mater.*, 28(46), 10182–10187.

Tang, D., Zhu, W., Wei, P., Zhou, H., Liu, Z., Yu, J., Zhao, W. (2015). Preparation and properties of $Zn_4Sb_{2.94}In_{0.06}$/ZnO composite thermoelectric materials. *J. Electron. Mater.*, 44, 1902–1908.

Tewolde, M., Fu, G., Hwang, D.J., Zuo, L., Sampath, S., Longtin, J.P. (2015). Thermoelectric device fabrication using thermal spray and laser micromachining. *J. Therm. Spray Technol.*, 25(3), 431–440.

Wang, S.Y., She, X.Y., Zheng, G., Fu, F., Li, H., Tang, X.F. (2012). Enhanced thermoelectric performance and thermal stability in b-Zn_4Sb_3 by slight Pb-doping. *J. Electron. Mater.*, 41, 1091–1099.

Wang, X., Veremchuk, I., Burkhardt, U., Bobnar, M., Bottner, H., Kuo, C.-Y., Chen, C.-T., Chang, C.-F., Zhao, J.-T., Grin, Y. (2018). Thermoelectric stability of Eu- and Na-substituted PbTe. *J. Mater. Chem. C.*, 6, 9482–9493

Weitzman, L.H. (1967). Etching bismuth telluride. Patent, US3338765A.

Wood, M., Kuo, J.J., Imasato, K., Snyder, G.J. (2019). Improvement of low-temperature *zT* in a Mg_3Sb_2 -Mg_3Bi_2 solid solution via Mg-vapor annealing. *Adv. Mater.*, 31(35), 1902337.

Wood, M., Imasato, K., Anand, S., Yang, J., Snyder, G.J. (2020). The importance of the Mg–Mg interaction in Mg_3Sb_2-Mg_3Bi_2 shown through cation site alloying. *J. Mater. Chem. A*, 8(4), 2033–2038.

Wu, Y., Ming, T., Li, X., Pan, T., Peng, K., Luo, X. (2014). Numerical simulations on the temperature gradient and thermal stress of a thermoelectric power generator. *Energy Convers. Manag.*, 88, 915–927.

Xia, X., Huang, X., Li, X., Gu, M., Qiu, P., Liao, J., Tang, Y., Bai, S., Chen, L. (2014). Preparation and structural evolution of Mo/SiO_x protective coating on $CoSb_3$-based filled skutterudite thermoelectric material. *J. Alloys Compd.*, 604, 94–99.

Xing, T., Song, Q., Qiu, P., Zhang, Q., Gu, M., Xia, X., Liao, J., Shi, X., Chen, L. (2021). High efficiency GeTe-based materials and modules for thermoelectric power generation. *Energy Environ. Sci.*, 14(2), 995–1003.

Xu, C., Liang, Z., Shang, H., Wang, D., Wang, H., Ding, F., Mao, J., Ren, Z. (2021). Scalable synthesis of n-type $Mg_3Sb_{2-x}Bi_x$ for thermoelectric applications. *Mater. Today Phys.*, 17, 100336.

Xue, L., Zhang, Z., Shen, W., Ma, H., Zhang, Y., Fang, C., Jia, X. (2019). Thermoelectric performance of Cu_2Se bulk materials by hightemperature and high-pressure synthesis. *J. Materiomics*, 5, 103–110.

Yang, C.L., Lai, H.J., Hwang, J.D., Chuang, T.H. (2013). Diffusion soldering of $Bi_{0.5}Sb_{1.5}Te_3$ thermoelectric material with Cu electrode. *J. Mater. Eng.*, 22(7), 2029–2037.

Yang, J., Liu, G., Shi, Z., Lin, J., Ma, X., Xu, Z., Qiao, G. (2017a). An insight into β-Zn_4Sb_3 from its crystal structure, thermoelectric performance, thermal stability and graded material. *Mater. Today Energy*, 3, 72–83.

Yang, J., Zhang, X., Ge, B., Yan, J., Liu, G., Shi, Z., Qiao, G. (2017b). Effect of Zn migration on the thermoelectric properties of Zn_4Sb_3 material. *Ceram. Int.*, 43, 15275–15280.

Yin, H., Christensen, M., Pedersen, B.L., Nishibori, E., Aoyagi, S., Iversen, B.B. (2010). Thermal stability of thermoelectric Zn_4Sb_3. *J. Electron. Mater.*, 39, 1957–1959.

Yin, L., Chen, C., Zhang, F., Li, X., Bai, F., Zhang, Z., Wang, X., Mao, J., Cao, F., Chen, X. et al. (2020). Reliable N-type $Mg_{3.2}Sb_{1.5}Bi_{0.49}Te_{0.01}$/304 stainless steel junction for thermoelectric applications. *Acta Mater.*, 198, 25–34.

Ying, P., He, R., Mao, J., Zhang, Q., Reith, H., Sui, J., Ren, Z., Nielsch, K., Schierning, G. (2021). Towards tellurium-free thermoelectric modules for power generation from low-grade heat. *Nat. Commun.*, 12(1), 1121.

Zhang, J.F., Yang, K., Deng, C.M., Deng, C.G., Liu, M., Dai, M.J., Zhou, K.S. (2014). Method for preparing thick nickel coating on surface of semiconductor material. Patent, CN104357784A.

Zhang, Q.H., Huang, X.Y., Bai, S.Q., Shi, X., Uher, C., Chen, L.D. (2016). Thermoelectric devices for power generation: Recent progress and future challenges. *Adv. Eng. Mater.*, 18(2), 194–213.

Zhang, J., Song, L., Pedersen, S.H., Yin, H., Hung, L.T., Iversen, B.B. (2017). Discovery of high-performance low-cost n-type Mg_3Sb_2-based thermoelectric materials with multi-valley conduction bands. *Nat. Commun.*, 8, 13901.

Zhang, J., Song, L., Iversen, B.B. (2019). Insights into the design of thermoelectric Mg_3Sb_2 and its analogs by combining theory and experiment. *Npj Comput. Mater.*, 5(1), 76.

Zhang, X., Bu, Z., Lin, S., Chen, Z., Li, W., Pei, Y. (2020a). GeTe thermoelectrics. *Joule*, 4(5), 986–1003.

Zhang, Z., Zhao, K., Wei, T.-R., Qiu, P., Chen, L., Shi, X. (2020b). Cu_2Se-based liquid-like thermoelectric materials: Looking back and stepping forward. *Energy Environ. Sci.*, 13, 3307–3329.

Zhao, D. and Tan, G. (2014). A review of thermoelectric cooling: Materials, modeling and applications. *Appl. Therm. Eng.*, 66(1–2), 15–24.

Zhao, D., Geng, H., Chen, L. (2012). Microstructure contact studies for skutterudite thermoelectric devices. *Int. J. Appl. Ceram. Technol.*, 9(4), 733–741.

Zheng, Z., Su, X., Deng, R., Stoumpos, C., Xie, H., Liu, W., Yan, Y., Hao, S., Uher, C., Wolverton, C. et al. (2018). Rhombohedral to cubic conversion of GeTe via MnTe alloying leads to ultralow thermal conductivity, electronic band convergence, and high thermoelectric performance. *J. Am. Chem. Soc.*, 140(7), 2673–2686.

Zhu, Q., Song, S., Zhu, H., Ren, Z. (2019). Realizing high conversion efficiency of Mg3Sb2-based thermoelectric materials. *J. Power Sources*, 414, 393–400.

Zou, T., Xie, W., Feng, J., Qin, X., Weidenkaff, A. (2015). Recent developments in β-Zn_4Sb_3 based thermoelectric compounds. *J. Nanomater.*, 642909.